Received: 8 November 2020 | Revised: 3 January 2021 | Accepted: 4 January 2021

DOI: 10.1002/nano.202000232

REVIEW

Nano Select WILEY

Recent advances of biomass carbon dots on syntheses, characterization, luminescence mechanism, and sensing applications

Ying Lou[1] | Xinyu Hao[1] | Lei Liao[1] | Kaiyou Zhang[1] | Shuoping Chen[1] | Ziyuan Li[1] | Jun Ou[1] | Aimiao Qin[1] | Zhou Li[2]

[1] Key Lab New Processing Technology for Nonferrous Metals & Materials Ministry of Education, College of Materials science and engineering, College of Environmental Science and Engineering, Guilin University of Technology, Guilin, China

[2] Beijing Institute of Nanoenergy and Nanosystems, Chinese Academy of Sciences, Beijing, China

Correspondence

Aimiao Qin, Key Lab New Processing Technology for Nonferrous Metals & Materials Ministry of Education, College of Materials science and engineering, College of Environmental Science and Engineering, Guilin University of Technology, Guilin, China.
Email: 592491245@qq.com

Zhou Li, Beijing Institute of Nanoenergy and Nanosystems, Chinese Academy of Sciences, Beijing 101400, China.
Email: zli@binn.cas.cn

Abstract

Carbon dots have attracted much attention due to their high fluorescence intensity, easy modification, good stability, and biocompatibility. However, the realization of low-cost mass production of high-quality carbon dots still faces great challenges. Biomass is of non-toxic and environmentally friendly organism, but a lot of biomass is treated as waste for burning and landfill at present, causing irreparable pollution to the environment. In fact, many biomass resources are ideal candidates for preparing carbon dots. This review focuses on carbon dots including carbon quantum dots (CQDs) and graphene quantum dots (GQDs) which using biomass as carbon source on the aspects of plants and their derivatives, animals and their derivatives and municipal waste. The characterization of the structure and composition of biomass carbon dots, the regulation of fluorescence color and the methods of improving quantum yield (QY) including heteroatom doping and surface modification are introduced in detail. Moreover, biomass carbon dots for detecting metal ions and non-metal molecules and their quenching mechanism are emphatically introduced in addition to summarizing the luminescence mechanism, and some promising prospects and challenges in this uplifting field are discussed.

KEYWORDS

biomass, carbon dots, luminescence mechanism, metal ions detection, quenching mechanism

1 | INTRODUCTION

Carbon mainly exists in the form of graphite, diamond, and carbon nanotubes in nature. In recent years, carbon materials have attracted extensive attention in energy, materials, and biology. For example, carbon nanotubes and graphene play a very vital role in optoelectronic materials, new energy resources, biomedical nanomaterials because of their excellent optoelectronic properties.[1] Due to the lack of proper bandgap, the application of carbon materials in optoelectronics is limited, especially in the field of luminescent materials.

In recent years, traditional carbon materials have developed into a novel fluorescent material-carbon dots through

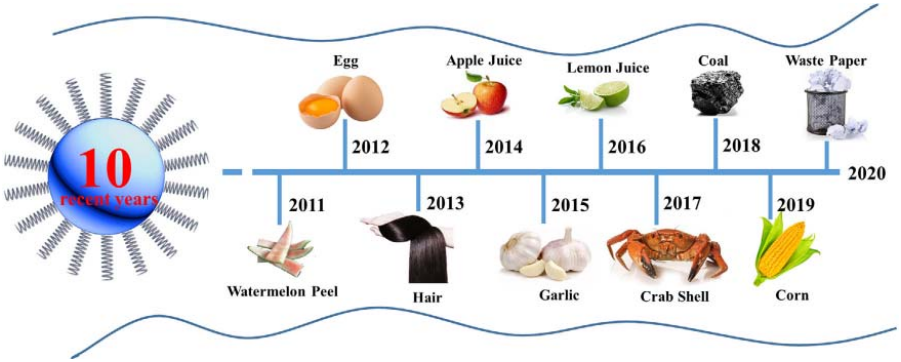

FIGURE 1 Development map of biomass carbon dots in recent ten years

the control of particle size and surface functionalization, which is different from two-dimensional (2D) graphene piece and one-dimensional graphene nanobelt.[2] As a novel quasi-zero-dimensional fluorescent nanomaterial, the movement of internal electrons of carbon dots in all directions is limited, showing a stronger quantum confinement effect, which makes them have great potential application value in materials, biology, medicine and new semiconductor devices attributing to its excellent optical and electrical properties.[3]

Up to now, various carbon sources have been developed to prepare carbon dots. However, many studies have paid more attention to the application of materials and ignored the cost, toxicity, and pollution of carbon sources. In fact, low-cost biomass, which is considered to be waste, have been converted into valuable carbon dots by some researchers due to its advantages of renewable, low pollution, and wide distribution. In recent years, researchers have used biomass such as plants and their derivatives,[4–10] animals their derivatives[11–14] and municipal waste[15–17] to produce biomass carbon dots (Figure 1).

Herein, this review will elaborate on the biomass carbon dots from carbon source and synthesis method, characterization, and properties, luminescence mechanism and application in sensing to meet the interest of relevant researchers in this field (Scheme 1). Furthermore, the prospects of biomass carbon dots are also presented.

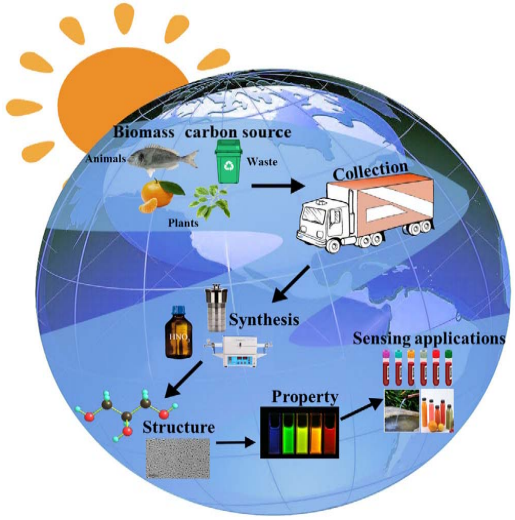

SCHEME 1 Schematic illustration of carbon sourse, synthesis method, structure, property and sensing applications for biomass carbon dots.

2 | CARBON SOURCE AND SYNTHESIS METHOD OF BIOMASS CARBON DOTS

2.1 | Carbon source

Biomass refers to all organisms produced by photosynthesis through atmosphere, water and land, including plant, and animal derivatives, industrial organic wastewater and municipal solid waste, etc. It is mainly composed of organic polymers, including carbon, hydrogen, and oxygen in chemical composition. Some biomass may also contain other elements such as nitrogen, sulfur, and sodium, so it has the general characteristics of organism and polymer. Biomass not only has the advantages of variety and wide distribution, but also has better biodegradability and regeneration. Therefore, it becomes an ideal carbon source for the preparation of carbon dots. Biomass carbon dots derived from different carbon sources and their properties are shown in Table 1.

TABLE 1 Biomass carbon dots prepared from different carbon sources and their properties

Types of biomass	Carbon source	Method	Product	Size [nm]	QY [%]	Color or emission [nm]	Ref
Plants and their derivatives	Gingko biloba	Microwave	CQDs	15–20	/	479	[4]
	Rice husk	Hydrothermal	CQDs	3.7 ± 1.4	15	469–552	[18]
	Orange waste peels	Hydrothermal	CQDs	2.9 ± 0.5	11.3	426	[73]
	Palm oil	Hydrothermal	CQDs	5–7	24.6	440	[71]
	Cane sugar	Solvothermal	CQDs	9.5 ± 1.9	5.2	/	[193]
	Green tea	Hydrothermal	CQDs	5	12	658	[22]
	Alkali lignin	Hydrothermal	CQDs	1.5–3.5	17.6	525	[194]
	Mushroom	Microwave	CQDs	20	/	506	[25]
	Potato starch	Ultrasonic	CQDs	3–5	10	515	[21]
	Larch wood	Hydrothermal	CQDs	3.28	/	434	[195]
	Ocimum tenuiflorum	Hydrothermal	Carbon Dots	1–3	11.5	405	[23]
	Cyanobacteria	Hydrothermal	CQDs	2.48	9.24	439	[24]
	Scindapsus leaves	Solvothermal	CQDs	2–6	/	458	[82]
	Latex	Hydrothermal	CQDs	3.4 ± 0.45	39.2	450	[72]
	Pomelo	Hydrothermal	CQDs	3	/	452	[74]
	Lemon juice	Hydrothermal	CQDs	3.1	10	482	[8]
	Beetroot	Hydrothermal	CQDs	5/8	6/5	450/520	[75]
	Lemon peel	Hydrothermal	CQDs	6–14	11	505	[196]
	Walnut shells	Pyrolysis	CQDs	3.4	/	520	[85]
	Orange pericarp	Hydrothermal	CQDs	1.4–3.8	2.88	524	[20]
	Lime juice	Hydrothermal	CQDs	7.6 ± 2.7	40	443	[28]
	Tea,Peanut Shell	Hydrothermal	CQDs	7–9	/	Blue	[127]
	Lignocellulosic	Microwave	CQDs	17.5	2.7	435	[197]
	Sugar beet	Pyrolysis	CQDs	0.9 ± 0.4	/	405	[86]
	Eichhornia crassipes	Hydrothermal	CQDs	1–2.5	/	459	[198]
	Sugarcane bagasse	Hydrothermal	GQDs	2.26	35.7	/	[199]
	Cotton Cellulose	Hydrothermal	GQDs	3.0–3.5	19.4	551	[200]
	Lignin	Hydrothermal	GQDs	20–25	12.4	545	[26]
	Lignin	Hydrothermal	GQDs	2–6	21	410	[27]
	Corn powder	Hydrothermal	GQDs	20–30	/	450	[201]
	Mango leaves	Microwave	GQDs	2–8	/	/	[202]
	Fenugreek seed	Hydrothermal	GQDs	5.6 ± 0.3	/	/	[203]
	Rice grains	Pyrolysis	GQDs	2–6.5	24	440	[87]
	Neem leaf	Hydrothermal	GQDs	5	41.2	440	[29]
	Durian	Hydrothermal	GQDs	2–6	6.8	601	[129]
	Rice Husk	Hydrothermal	GQDs	3–6	15	/	[204]
Animals and their derivatives	Hair	Hydrothermal	CQDs	2–8	10.7	415	[13]
	Roasted fish	Hydrothermal	CQDs	2.73 ± 0.48	/	348	[37]
	Collagen	Hydrothermal	CQDs	1.25 ± 0.21	15	510	[38]
	Cow milk	Hydrothermal	GQDs	2.8	8	415	[39]
	Cow milk	Microwave	GQDs	5	25	/	[40]
	Silk Fibroin	Microwave	CQDs	5.4 ± 0.9	15	Blue	[41]
	Crab Shell	Microwave-hydrothermal	CQDs	4.0 ± 0.7	19.84	Blue	[12]

(Continues)

TABLE 1 (Continued)

Types of biomass	Carbon source	Method	Product	Size [nm]	QY [%]	Color or emission [nm]	Ref
	Gelatin	Hydrothermal	CQDs	1.7	31.6	430	[205]
	Honey	Hydrothermal	CQDs	2	19.8	435	[206]
	Egg	Plasma	Carbon Dots	2.15	5.96	420	[11]
	Wool	Pyrolysis	CQDs	6.05±1.67	22.5	402	[207]
Municipal waste	Whey	Pyrolysis	CQDs	4	11.4	425	[88]
	Aqua mesophase pitch	Hydrothermal	CQDs	2.8	27.6	420	[208]
	Sugarcane bagasse pulp	Chemical oxidation	CQDs	4.1 ± 0.17	18.7	438	[54]
	Chinese ink	Chemical oxidation	CQDs	5	78	482	[53]
	Cane molasses	Hydrothermal	GQDs	1.1–3.2	21.3	440	[30]
	Wine lees	Hydrothermal	CQDs	10	6	433 ± 13	[209]
	Vehicle-generated toxic pollutants	Hydrothermal	CQDs	4.2	5.63	396	[51]
	Anthracite	Chemical oxidation	CQDs	/	/	/	[56]
	Ice-biryani	Pyrolysis	CQDs	2–5	41	432	[52]
	Waste paper	Hydrothermal	CQDs	1–5	/	420	[15]
	Coke powder	Hydrothermal	CQDs	2.0–2.5	34.2	/	[59]
	Lignite	Chemical oxidation	CQDs	1.72	/	450	[58]
	Coal tar pitch	Solvothermal	CQDs	5.17 ± 0.95	/	/	[83]
	Coke	Ultrasonic	CQDs	/	9.2	410	[61]
	Peat	Pyrolysis	CQDs	/	/	426	[89]
	Styrene soot	Ultrasonic	CQDs	3	/	480	[210]
	Coke	Chemical oxidation	CQDs	5	15.8	510	[60]
	Organic waste	Photoinduced chemical reduction	CQDs	2		450	[211]
	Coal-Tar-Pitch	Ultrasonic	GQDs	1.7	2.37	445	[63]
	Coke	Electrochemical exfoliation	GQDs	2.9	19.2	440	[62]
	Coal	Chemical oxidation	GQDs	4–6	9.12	Blue	[57]
	Deoiled asphalt	Microwave	GQDs	1–6	16.4	442	[64]
	Petroleum Asphalt	Chemical oxidation	GQDs	2.44	16.1	Green	[65]
	Asphaltene	Chemical oxidation	GQDs	1.3–3.7	18	Green	[128]
	Anthracite Coal	Ultrasonic	GQDs	3	28	Blue	[55]
	Sewage Sludge	Hydrothermal	GQDs	/	10.3	/	[212]
	Anthracite Coal	Chemical oxidation	GQDs	4.5 ± 1.2	/	Green to orange-red	[16]
	Coal	Chemical oxidation	GQDs	10	1.8	Yellow	[17]

2.1.1 | Plant and their derivatives

Plants are rich in sugar, vitamin, and amino acid, as well as pectin, cellulose, hemicellulose, starch, and some free metal ions. At present, some study has been reported on carbon dots which obtained from various plants and their derivatives. For most carbon dots derived from plants or their derivatives as carbon sources, the particle size of carbon dots is usually less than 10 nm. For example, the carbon quantum dots (CQDs) with the size of 3.7 nm derived from rice husk[18] was obtained by adjusting the hydrothermal conditions to influence the carbonation reaction and their quantum yield (QY) was 15%. Niu et al.[19] prepared carbon dots with the QY of 1.68% and 2.47% in water and solid state, respectively, which were both less than 10 nm in diameter. Du et al.[20] synthesized water-soluble CQDs from orange pericarp with a size ranging from 1.4 to 3.8 nm, and the QY is 2.88%. Using potato starch[21] as carbon source, CQDs with abundant oxygen groups were synthesized by ultrasonic method, the particle size and QY were 3–5 nm and 10%, respectively. At the same time, green tea,[22] ocimum tenuiflorum,[23] and cyanobacteria,[24] etc. were also used as carbon source to synthesize carbon dots. However, not all biomass carbon dots are less than 10 nm in size. The diameter of ginkgo biloba[4] CQDs by microwave could reach 15–20 nm, and the CQDs synthesized by microwave using mushrooms[25] as carbon source were also between 10 and 20 nm. It cannot be inferred that the size is only related to the synthesis method. Temerov et al.[26] obtained graphene quantum dots (GQDs) from lignin by hydrothermal method is 20–25 nm, and the highest QY can reach 12.4%. Similarly, using lignin as carbon source, Ding et al.[27] synthesized GQDs with a size of only 2–6 nm, while the QY can reach 21%. As for the synthesis method, both of the two adopted the treatment method of first ultrasonic and then hydrothermal. The difference is that the former was treated with ultrasonic for 10 minutes in alkaline environment while the latter was treated for 2 hours in acidic environment. Therefore, it is speculated that the formation of carbon dots may be related to the pH of the system and the ultrasonic time.

Unlike small molecules, biomass materials cannot quantitatively control the content of certain compounds to form carbon dots, so the QY of carbon dots derived from biomass would be slightly less efficient than that of the small molecules. However, this does not mean that high-quality carbon dots cannot be produced on a large scale from biomass. To solve this problem, many researchers have adopted various measures to increase the QY of biomass carbon dots. The QY could be as high as 40% when nitrogen was doped[28] to prepare carbon dots using lime juice. Meaningly, Roy et al.[29] prepared nitrogen-doped GQDs and fluorine-doped GQDs from plant leaves as carbon sources with a QY of 41.2% and 38.9%, respectively. Our group[30] prepared cane molasses GQDs and modified their surface defects with polyethene glycol, the QY was twice as high as that of the unpassivated GQDs. These examples show that the heteroatom doping or surface modification can improve the QY of carbon dots to some extent. Besides, many other plant derivatives used to prepare carbon dots were also reported including rose-heart radish,[31] beer,[32] coriander leaves,[33] onion,[34] garlic,[10] banana juice,[35] linseed,[36] and so on.

2.1.2 | Animal and their derivatives

Most animals and their derivatives contain more amino acids, proteins and trace elements compared with plants and their derivatives. Therefore, it is not rare to prepare carbon dots from animals or animal derivatives, and the size of which is basically less than 8 nm. For example, blue fluorescent CQDs with a size of 2–8 nm and a QY of 10.75% were obtained by the hydrothermal treatment of hair based on the fact that the main component of hair is keratin[13]. Similarly, Sun et al.[14] also used hair as carbon source to prepare S,N-CQDs. The CQDs prepared from roasted fish[37] have the size of about 2.73 nm, and could be used for the detection of protease. Hydrothermal treatment of collagen[38] could even create CQDs as small as 1.25 nm for cellular imaging. Besides, it has to be mentioned that the QY of hydrothermal synthesis of GQDs using milk[39] as precursor is 8%, while the GQDs from milk synthesized by microwave method can reach 25% and could be used for drug loading and release.[40] Accordingly, Ko et al.[41] reported that blue fluorescent CQDs with the size of about 5.4 nm could be synthesized in a short time by microwave irradiation using silk fibroin as carbon source. The magnetic fluorescent CQDs with a diameter of 4 nm could be obtained in just 10 minutes by microwave-assisted pyrolysis of crab shell[12] with three different transition metal ions. Using crab shell as carbon source can not only achieve waste reuse, but also prepare high-quality CQDs for targeted biological imaging and drug delivery. What's more interesting is that Essner et al.[42] used urine from different people as carbon source to synthesize "pee-dots", and the size of pee-dots directly reflected the dietary habits of urine donors. Moreover, many other animal derivatives used to prepare carbon dots were also reported including wool,[43] cow manure,[44] goose feathers,[45] silkworm chrysalis,[46] eggshell,[47] and so on. However, the number of reports on the preparation of carbon dots from animals and their derivatives is less than that from plants and their derivatives since that the type and quantity of available animal derivatives are not so many as those of plant derivatives. However, this does not hinder the value of preparing

high-quality carbon dots using animals and their derivatives as carbon sources.

2.1.3 | Municipal waste

Municipal waste refers to industrial solid waste, wastewater, and garbage, among which the industrial solid waste is an extensive biomass resource, including the waste residue of food processing, brewing, textile, and other industries with strong biodegradability. According to the relevant urban survey data, industrial organic solid waste accounted for 11% of the total industrial solid waste.[48,49] Wastewater includes domestic wastewater and industrial wastewater, and the exploitation of industrial organic wastewater can obtain double benefits of energy and environmental protection.[50] Garbage contains a large amount of biomass resource, which is easy to be centrally used because of its complete collection, transportation, and storage system. Therefore, more and more research has been reported on carbon dots prepared using municipal waste as carbon source.

With the rapid growth of the number of vehicles, the threat of vehicle-generated toxic pollutants to the environment becomes more and more serious. Many researchers were inspired to convert exhaust pollutants into valuable carbon dots. Devi et al.[51] reported that a simple hydrothermal method to yield CQDs with an average size of 4.2 nm using soot as carbon source. The recycling of kitchen waste can reduce the amount of organic matter entering the landfill, reduce the generation of odor and landfill leachate, and avoid the adverse impact of excessive moisture on waste incineration. Milrad et al.[52] were inspired to use ice-biryani from kitchen waste as carbon source to obtain blue fluorescent carbon dots with a size of 2–5 nm by pyrolysis, and a high QY of 41% was achieved at the same time. Besides, the QY of 5 nm CQDs prepared from Chinese ink[53] could reach as high as 78%. Similarly, uniformly distributed carbon dots could also be produced by using sugarcane bagasse pulp[54] and cane molasses[30] as carbon sources. Industrial solid waste accounts for a significant part of municipal waste and the reports about coal, coke, and asphalt are common. Coal is mainly composed of carbon, hydrogen, oxygen and a small amount of nitrogen, sulfur or other elements. According to its different carbonization degree, it can be divided into peat, lignite, bituminous coal (raw coal), anthracite, respectively. The carbonization degree of anthracite is the highest and that of peat is the lowest. Sulfur is one of the common impurities in coal, which usually appears in the combustion products of coal in the form of sulfides. In some countries, such as the United States, regulations have been established to control sulphide emissions. Therefore, many researchers have converted coal into more valuable, environmentally friendly and non-toxic carbon dots for various applications. Sasikala et al.[55] used anthracite coal to synthesize blue fluorescent GQDs with an average size of 3 nm and a QY of 28% by ultrasonic method. Also using anthracite as raw material, Ye et al.[16] adjusted the band gap of the synthesized GQDs by cross-flow ultrafiltration and controlling the reaction temperature respectively, which made the GQDs emit different fluorescence colors from green to orange. The highest QY of the synthesized GQDs can even be as high as 52%. Similarly, Jia et al.[56] changed the band gap width of the synthesized CQDs by controlling the concentration of hydrogen peroxide, thereby color adjustment of the CQDs can be realized. According to these reports, it can be seen that anthracite has the potential to synthesize GQDs with high QY from blue to orange and even red. Tang et al.[57] used six different kinds of coal as raw materials to prepare GQDs. It was found that the size of GQDs synthesized from anthracite was the largest, and the lower the carbonization degree of coal was, the smaller the diameter of the synthesized GQDs would be. Using lignite[58] with slightly lower carbonation as raw material, the blue CQDs with emission wavelength at 450 nm were obtained by chemical oxidation and the size was only 1.72 nm. The results also confirmed Tang's report. Coke is a kind of solid fuel. It is obtained from coal by dry distillation at about 1000°C. The main component is fixed carbon, followed by ash, which contains little volatilization and sulfur. The carbon dots using coke as carbon source have been synthesized by various methods including hydrothermal,[59] chemical oxidation,[60] ultrasonic,[61] electrochemical exfoliation,[62] and so on. The size and QY of carbon dots prepared by different methods are also different. Among them, the carbon dots prepared by hydrothermal method using coke powder[59] as carbon source have higher QY than that of other methods, which could reach 34.27%. We speculate that this is because the coke powder may have more contact area exposed to the outside during the reaction, making the reaction more sufficient. Asphalt is a dark brown complex mixture composed of hydrocarbons with different molecular weight and their non-metallic derivatives. Pitch can be divided into coal tar pitch, petroleum asphalt, and natural pitch, among which coal tar pitch is a by-product of coking, petroleum asphalt is the residue of crude oil after distillation and natural asphalt is mostly stored in the underground. At present, most reports on the preparation of carbon dots with asphalt as carbon source were mainly coal tar pitch and petroleum asphalt. Most carbon dots with blue and even green fluorescence produced from pitch were very small and thin GQDs with size no

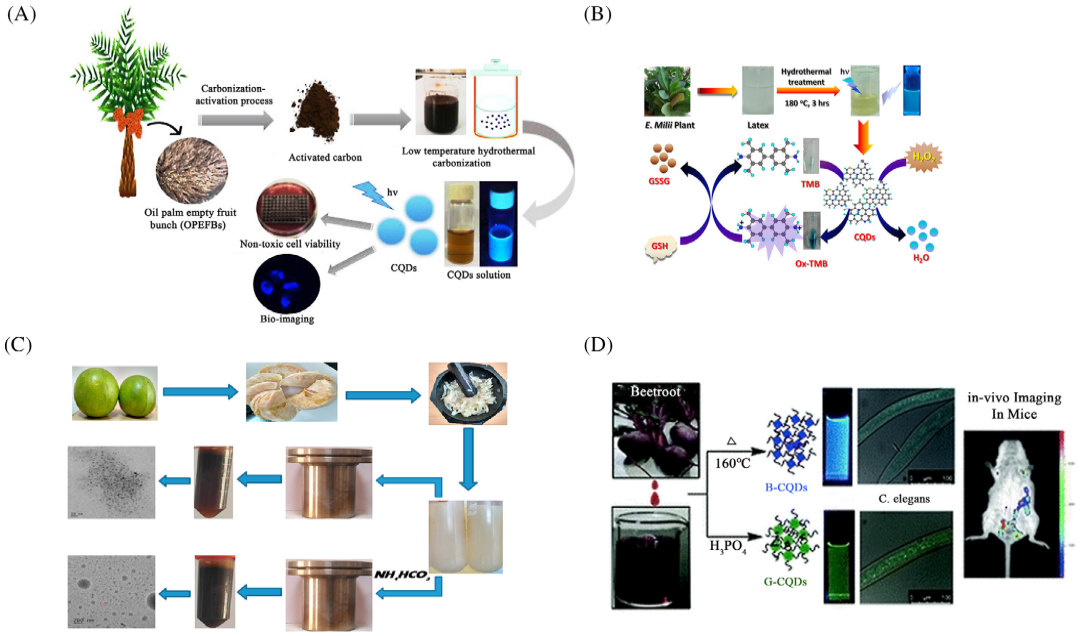

FIGURE 2 Schematic illustration of preparation of biomass carbon dots by hydrothermal methods from (A) oil palm, (B) latex of Euphorbia milli, (C) citrus grandis and (D) beetroot. Reproduced with permission.[71] Copyright 2020, Elsevier. Reproduced with permission.[72] Copyright 2019, American Chemical Society. Reproduced with permission.[74] Copyright 2018, Elsevier. Reproduced with permission.[75] Copyright 2018, Royal Society of Chemistry

more than 6 nm, and the QY of these GQDs was generally not very high. Many carbon dots from coal have been synthesized by only one process, including ultrasound,[63] microwave,[64] and chemical oxidation.[65]. Besides, other municipal waste including gas soot,[66] waste chimney oil,[67] and food waste.[68] has also been reported to be used to prepare carbon dots.

2.2 | Synthesis method

The synthesis method of biomass carbon dots can be divided into physical synthesis and chemical synthesis according to whether the chemical reaction takes place or not. Physical synthesis mainly includes vapor deposition, grinding, ultrasonic synthesis, molecular epitaxy, and photoetching. Compared with the chemical synthesis, the physical synthesis may cause many defects on the material surface, the destruction of the morphology and the easy contamination of the material itself in the preparation process. Therefore, chemical synthesis has been more used by researchers. Other preparation methods of biomass carbon dots have been discussed in detail in some reports.[69,70] The following will focus on the different chemical synthesis methods including hydrothermal method, solvothermal method, chemical oxidation method and pyrolysis method.

2.2.1 | Hydrothermal and solvothermal method

Hydrothermal synthesis is a chemical reaction method in aqueous solution under the conditions of temperature of 100 ~ 1000 °C and pressure of 1 MPa ~ 1 GPa. The advantage of hydrothermal synthesis is that the ions are evenly mixed in aqueous solution, so the product has high purity, good dispersion, and easy particle size control. Some reports used biomass such as palm oil[71] and latex[72] as carbon source to directly dissolve in ultrapure water and then proceeding with hydrothermal reaction (Figure 2A and 2B) to prepare CQDs, the sizes of which were about 6 and 3.4 nm, respectively, and both of them have good dispersibility. Besides, it is reported

that the CQDs prepared from orange waste peels[73] were well dispersed and the average diameter was about 2.9 nm. Undoped CQDs and nitrogen-doped CQDs were prepared by hydrothermal method using citrus grandis as carbon source (Figure 2C) [74], the results showed that the average particle size of undoped CQDs is only 3 nm, while the nitrogen-doped CQDs is even up to 70 nm, indicating hydrothermal is one of important methods for adjusting the size of carbon dots. Similarly, different carbon dots without any treatment and with phosphoric acid treatment were prepared by using sugar beet root[75] extract as carbon source. It was found that blue and green fluorescent carbon dots could be obtained (Figure 2D), showing that hydrothermal is also one of the crucial ways to adjust the color of carbon dots. Besides, other biomass including grass,[76] pseudo-stem,[77] Hongcaitai,[78] ocimum sanctum,[79] pyrus pyrifolia,[80] Lantana camara berries[81] also involved the hydrothermal method to prepare carbon dots.

Solvothermal method is developed based on hydrothermal method. It differs from hydrothermal method in that the solvents used are organic solvents rather than water. Under liquid phase or supercritical conditions, the reactants dispersed in the solution become more active and the products are formed slowly. The process is relatively simple and easy to control, which can effectively prevent the volatilization of toxic substances and prepare air-sensitive precursors in closed systems. However, the disadvantages of the method are low yield, insufficient product purity, and unsatisfactory uniformity of product size and morphology. Generally speaking, hydrothermal has no negative effect on the properties of materials, but solvothermal has a significant influence on the properties of materials due to different solvents, so hydrothermal method is more common than solvothermal method in the synthesis. However, this does not mean that solvothermal method is not suitable for the preparation of biomass carbon dots. Using scindapsus leaves[82] (Figure 3A) and coal tar pitch[83] (Figure 3B) as carbon sources, ethanol and DMF were used as solvents to perform solvothermal reactions to obtain CQDs with quantum sizes of 2–6 nm and 5.17 ± 0.95 nm, respectively. Li et al.[84] also prepared near-infrared luminescent carbon dots by simple solvothermal method using spinach as carbon source and ethanol as solvent.

The fundamental difference between hydrothermal and solvothermal methods is that the supersaturation of biomass carbon source in water or other solvents, which affects the formation of crystal nucleus and crystal growth. The formation of high supersaturation in a short time is beneficial to the formation of crystal nucleus, which will affect the size of carbon dots. Therefore, it is very crucial to choose a suitable solvent environment for the preparation of biomass carbon dots and the regulation of its properties.

2.2.2 | Other methods

In addition to the two methods introduced above, chemical oxidation and pyrolysis methods have also been reported for the preparation of carbon dots from biomass. Chemical oxidation is the method in which the oxidant oxidizes the target by losing electrons. The advantages of this method are mild reaction conditions, easy to control, convenient operation and high selectivity. However, some oxidants are not only expensive but also pollute the environment. At present, there are also some reports on the preparation of carbon dots using biomass as carbon source by chemical oxidation. The CQDs with the QY up to 78% were obtained by chemically oxidizing nanosheets prepared from Chinese ink in a mixed solution of sulfuric acid and nitric acid (Figure 3C). In this report, the other three kinds of CQDs doped with heteroatoms were also obtained and applied to detect metal ions.[53] Tang et al.[57] synthesized GQDs by dissolving the coal in sulfuric acid and nitric acid. Also taking coal as the carbon source, Jia et al.[56] used hydrogen peroxide as the oxidant to obtain CQDs powder after simple operations such as centrifugal, filtration, and dialysis. The band gap of the CQDs was adjusted by changing the concentration of hydrogen peroxide, thus changing the luminescent color of the CQDs. Pyrolysis is the process of thermal decomposition of organic material under anoxic condition. Carbon dots with different sizes and properties can be prepared by pyrolysis under different conditions. The method is simple to operate and continuous production can be achieved. The ice-biryani[52] that had been ground into fine powder were carbonized at 250°C for about 24 hours. Finally, the higher purity CQDs were obtained under neutral conditions after dialysis. CQDs were synthesized from the dehydrated walnut shells which were carbonized at 1000 °C for 25 minutes in N_2 atmosphere.[85] Other studies have also been reported on the preparation of carbon dots by pyrolysis using different biomass as carbon source, such as sugar beet,[86] rice grains,[87] whey,[88] peat,[89] chia seeds,[90] and eleusine coracana (Figure 3D).[91] The blue fluorescent CQDs with the particle size of 0.9 ± 0.4 nm was prepared by using sugar beet[86] as carbon source. Using rice grains[87] as carbon source, GQDs with a size of 2–6.5 nm were obtained by controlling the heating time from 3 to 10 minutes at the same temperature. The results showed that the emission position of the GQDs prepared by pyrolysis method shifted to red, and the QY increased from 16% to 24% with the extension of heating time. We inferred that different heating time may affect the nucleation velocity of the GQDs and thus leads to the different performance of GQDs. In addition, Devi et al.[88] directly pyrolyzed whey to obtain uniformly dispersed blue fluorescent CQDs with a QY of 11.4% and applied it to the detection of selenite.

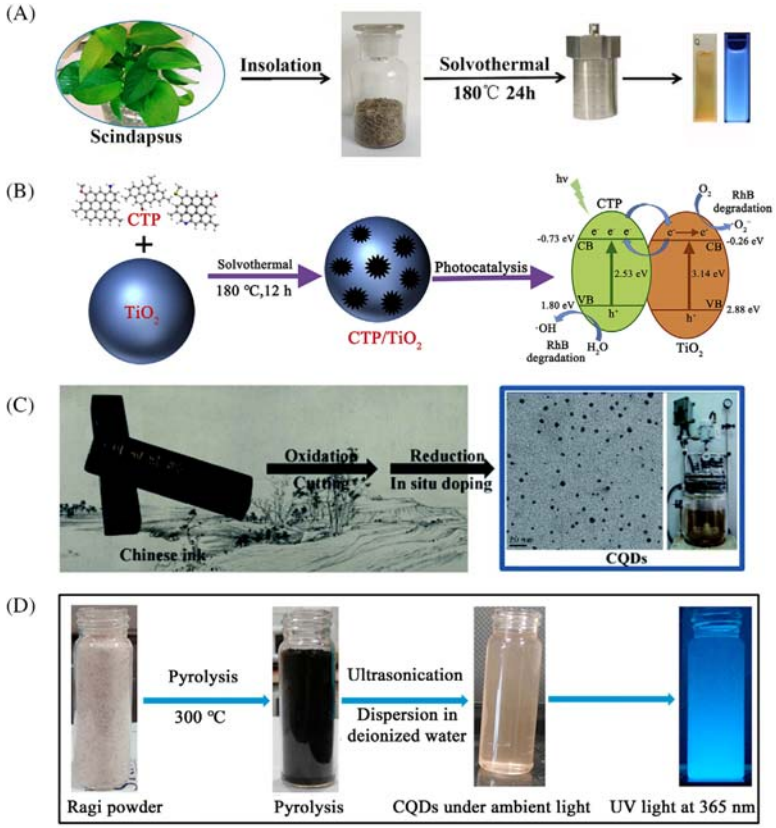

FIGURE 3 Schematic illustration of preparation of biomass carbon dots by solvothermal methods from (A) scindapsus, (B) coal tar pitch, by chemical oxidation from (C) Chinese ink, and by pyrolysis methods from (D) eleusine coracana. Reproduced with permission.[82] Copyright 2019, WILEY-VCH Verlag GmbH. Reproduced with permission.[83] Copyright 2019, Elsevier. Reproduced with permission.[53] Copyright 2014, Royal Society of Chemistry. Reproduced with permission.[91] Copyright 2019, Elsevier

2.3 | Product yield of biomass carbon dots

The product yield (PY) of biomass carbon dots can be affected more or less due to the complexity of biomass composition. For example, Park et al.[92] used food-waste as carbon source to prepare carbon dots by ultrasonication, but other by-products were also produced during the reaction, the PY was only 1.2%. Hsu et al.[93] synthesized fluorescent carbon dots with blue, green, yellow and red emission by pyrolysis using coffee grounds as carbon source and the PY was 12%–15%. Jones et al.[90] also used pyrolysis to extract more than 5 times the carbon dots from the same pyrolysis product using chia seeds as carbon source, thereby improving the PY (reach to 10%). The CQDs with the PY of 76.9 wt% were obtained by mild oxidation ($NaOH/H_2O_2$ solution) from biomass by Jing et al.[94] At present, there is still no significant breakthrough in PY for most biomass carbon dots, which limits its commercial application to a certain extent. Therefore, the research on improving the PY of biomass carbon dots is still urgent.

3 | BASIC CHARACTERIZATION AND PROPERTIES OF BIOMASS CARBON DOTS

3.1 | Structure and composition of biomass carbon dots

The size of carbon dots in three dimensions is no more than twice the exciton Bohr radius of their corresponding semiconductor materials, which is generally spherical or quasi-spherical, and the diameter is often between 2–20 nm. Due to its small size, it is difficult to characterize the structure and morphology of quantum dots through the

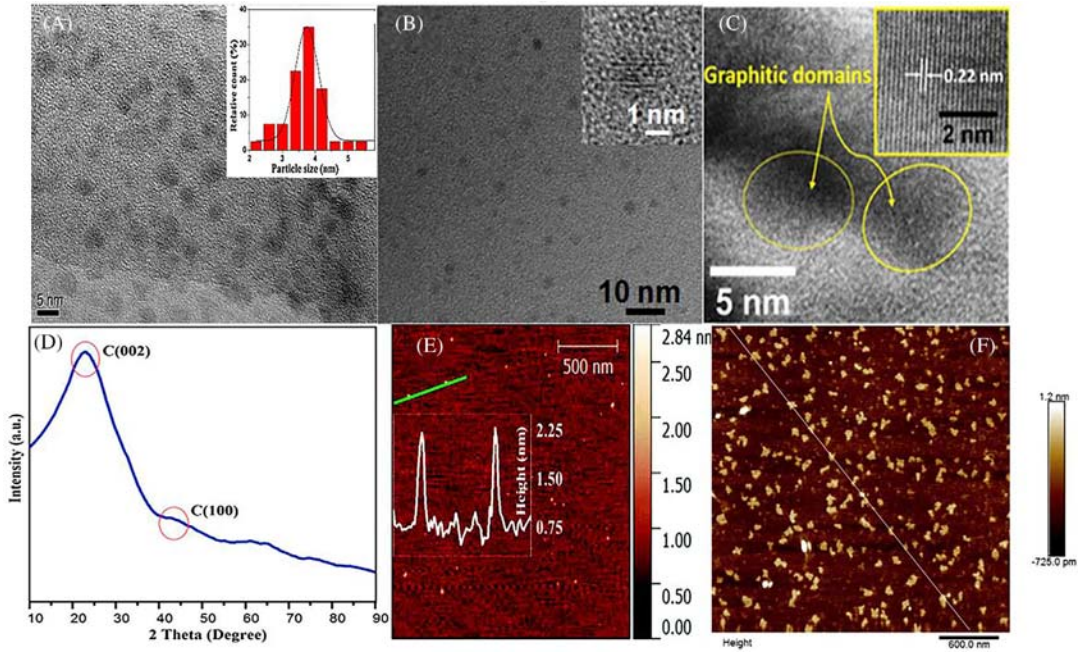

FIGURE 4 A, TEM image of carbon nanodots from bamboo leaves (inset: size distribution), (B) TEM image of N,P-CQDs from ink (Inset: HRTEM image), (C) TEM image of CQDs from Aegle marmelos leaves (Inset: HRTEM image), (D) XRD patterns of CQDs from eleusine coracana, (E) AFM image of GQDs from lignin and (F) AFM image of PN-CQDs from sucrose. Reproduced with permission.[95] Copyright 2014, Elsevier. Reproduced with permission.[99] Copyright 2018, MDPI. Reproduced with permission.[100] Copyright 2018, Elsevier. Reproduced with permission.[91] Copyright 2019, Elsevier. Reproduced with permission.[102] Copyright 2019, Royal Society of Chemistry. Reproduced with permission.[103] Copyright 2019, Springer Wien

scanning electron microscope (SEM), so it is necessary to characterize the morphology of quantum dots at relatively high multiples utilizing transmission electron microscope (TEM). The lattice stripes can be observed under high-resolution transmission electron microscope (HRTEM), thus determining the crystal plane corresponding to the carbon dots and the auxiliary analysis is often carried out with the aid of of X-ray diffraction (XRD). Atomic force microscopy (AFM) is used to obtain the information of surface morphology and roughness. In other words, the thickness of carbon dots can be measured by AFM to determine whether the carbon dots belong to CQDs or GQDs. Generally, GQDs have only a few graphite layers. Moreover, the composition of carbon dots can be further analyzed by Fourier transform infrared (FT-IR), X-ray photoelectron spectroscopy (XPS), etc.

3.1.1 | Structure of carbon dots

TEM is the most intuitive way to determine whether the material is quantum dots or not by characterizing the size and morphology of the material, and almost all reports about quantum dots involve TEM characterization. Many examples showed that the morphology of carbon dots prepared from biomass was usually spherical or quasi-spherical, such as bamboo leaves (Figure 4A),[95] cherry tomatoes,[96] cigarette filters,[97] hair[13] and, etc. Most biomass carbon dots were no more than 10 nm in size, and only a few were slightly larger. It is speculated that this may be related to the preparation conditions (reaction time, temperature, pH, etc.). To further determine the structure of carbon dots, HRTEM is used to observe the distance between light and dark stripes, and then compare it with the standard crystal plane spacing to determine which crystal plane it belongs to. The biomass carbon dots would possess good crystallinity if the clear lattice fringe was obtained from HRTEM. The Ph-Y-CQDs-500 from biomass tar clearly showed the lattice fringe, suggesting its crystalline nature.[98] The average size of CQDs prepared by hydrothermal method using apple juice[5] as carbon source was 2.8 nm, and the crystal plane spacing was 0.205 nm, which corresponds to the (102) crystal plane of sp^2

graphitic carbon. The uniformly dispersed CQDs-120 synthesized with Eleocharis dulcis[99] as a carbon source has a crystal plane spacing of about 0.34 nm, which corresponds to the (002) crystal plane of graphitic carbon (Figure 4B). Aegle marmelos leaves[100] were used to synthesize blue fluorescent CQDs with a lattice parameter of 0.22 nm corresponding to (100) graphite lattice planes (Figure 4C).

To further analyze the structural characteristics of carbon dots, XRD is often used in addition to HRTEM. Using Eleusine coracana[91] as the carbon source to obtain CQDs, the results of XRD showed that the diffraction peaks of CQDs at $2\theta = 25°$ and $2\theta = 42°$ correspond to (002) and (100) planes respectively, indicating that the synthesized CQD is essentially amorphous, which may be caused by the attachment of functional groups on the carbon surface (Figure 4D). The wide peak at 21.1° of CQDs prepared with jackfruit[101] as carbon source corresponds to the (002) plane, and a interlayer spacing gap of 0.09 nm existed between carbon dots and graphite, indicating that the crystallinity of carbon dots was not ideal, which attributed to the generation of more oxygen-containing groups. Similarly, the crystallinity of CQDs prepared with lemon juice[6] as carbon source was affected by the oxygen-containing functional groups on the surface. Therefore, the surface functional groups of carbon dots had influence to some extent on the crystallinity or amorphous structure.

Graphene can be divided into single layer, double layer, and multilayer according to its thickness. The standard thickness of single-layer graphene is 0.334 nm and no more than 0.4 nm; Double-layer graphene refers to a 2D carbon material composed of two layers of benzene ring structure (that is, hexagonal honeycomb structure) periodically and closely packed carbon atoms stacked in different stacking methods with a thickness of 1–2 nm; multilayer graphene refers to a benzene ring structure with more than 10 layers and a thickness of less than 10 nm. AFM can obtain surface morphology and structure information and surface roughness information with nanometer resolution. The thickness of GQDs synthesized from lignin[102] was 1.7 nm, which was equivalent to 2–4 layers of graphene (Figure 4E). The thickness of PN-CQDs synthesized from sucrose[103] was 0.7–3.5 nm (Figure 4F). The thickness of RH-GQDs synthesized with rice husk[104] was about 1.2–1.6 nm, corresponding to 2–3 layers of graphene. Overall, the thickness and material type of biomass carbon dots including CQDs and GQDs can be more accurately located with the help of AFM.

3.1.2 | Composition of carbon dots

FI-IR is one of the essential methods for the characterization of substances, which can provide a lot of information about functional groups and can help to determine some or even all molecular types and structures. XPS is a surface analysis technique, which is mainly used to characterize the surface elements and their chemical states of materials. Carbon dots from biomass was rich in a variety of organic compounds and have multiple functional groups on the surface, so FI-IR and XPS are often used to qualitatively analyze the composition and surface properties of biomass carbon dots.

The FI-IR characterization of CQDs synthesized with quince fruit[105] as carbon source showed that it contained C = C from polycyclic aromatic hydrocarbons besides the vibrations of -OH, -CH_2, and -CH_3, and the stretching vibration of C = O and C = C from carboxylic acids, which was closely related to quinic acid, malic acid, and ascorbic acid[106] in quince fruit. For the XPS analysis of the CQDs, in addition to the C element accounting for more than half of the proportion, there were also non-negligible O elements and a very small amount of N and S elements. No other elements were deliberately introduced during the preparation of carbon dots by the microwave method, which indicated that quince fruit itself contains N and S. Furthermore, the data obtained from the fine spectrum analysis of each element obtained by XPS was consistent with the FT-IR data. CQDs synthesized with salep[107] as carbon source showed typical O-H absorption band, C-O stretching vibration band at 1109 cm^{-1}, C = O stretching vibration band at 1707 cm^{-1}, and asymmetric and symmetric stretching vibration of C-O-C by FI-IR, which indicated the presence of carboxylic acid and other oxygen-containing functional groups on the synthesized CQDs. The CQDs prepared with rice residue[108] as carbon source contained characteristic peaks of C-N, C = O, C-O-C and C-O in the FI-IR spectrum (Figure 5A). The XPS spectra of C, N, and O (Figure 5B-5E) were then obtained, and the results were consistent with the FT-IR analysis. According to numerous reports on the FT-IR and XPS analysis of biomass carbon dots, a large proportion of carbon dots contain -OH, C-H, C = O, C = C, and generally contain more or less N and S elements besides C and O elements.

3.2 | Optical properties

3.2.1 | Absorbance

Biomass carbon dots usually have obvious absorption in the ultraviolet region of 200–400nm. The ultraviolet absorption spectrum is produced by the transition of the valence electron energy level in the molecule, and there are only two kinds of absorption in the ultraviolet region: π-π* transition and n-π* transition.

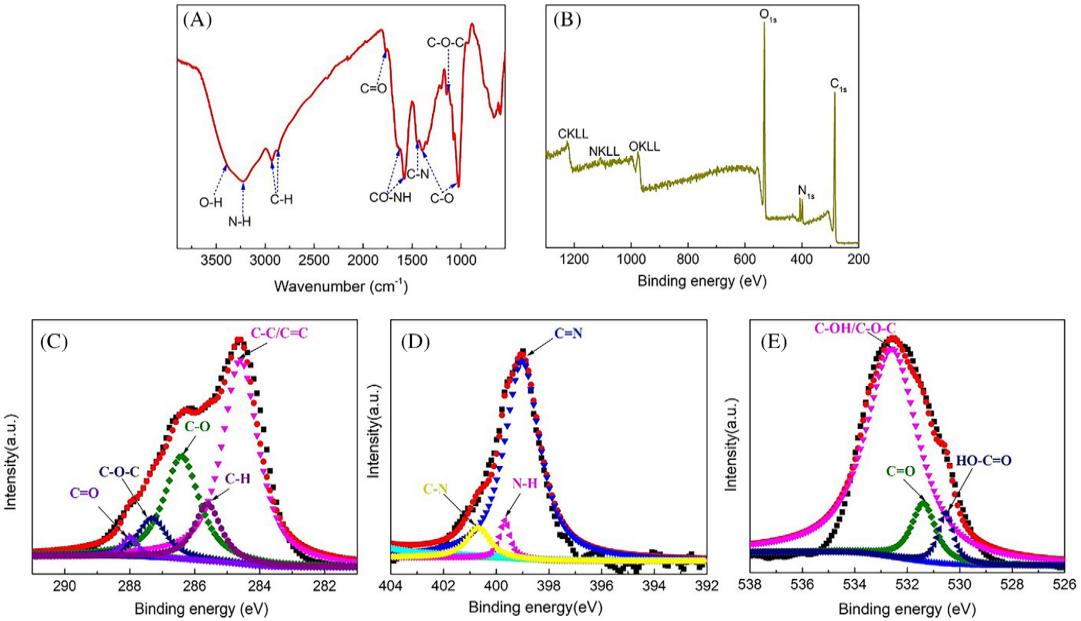

FIGURE 5 A, FTIR spectrum of the N-CQDs from rice residue, (B) XPS survey spectrum, (C) High-resolution C1s peaks and fitting curves, (D) High-resolution N1s peaks and fitting curves and (E) High-resolution O1s peaks and fitting curves. Reproduced with permission.[108] Copyright 2019, Elsevier

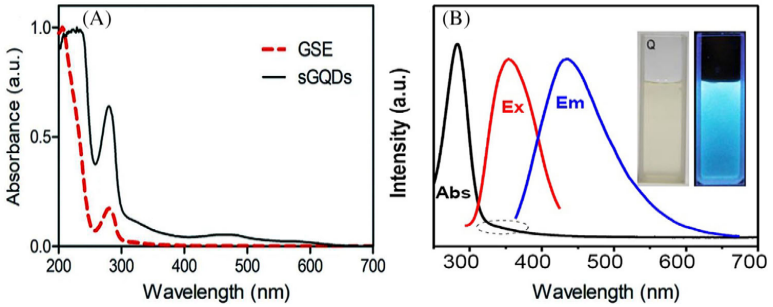

FIGURE 6 A, UV-vis absorption spectrum of GQDs from grape seed, (B) UV–vis absorption, photoluminescence excitation, and emission spectra of N-CQDs from watermelon juice (inset: photographs of N-CQDs under daylight and 365 nm UV light lamp). Reproduced with permission.[109] Copyright 2017, Nature Publishing Group. Reproduced with permission.[112] Copyright 2018, Elsevier

The strong characteristic absorption of GQDs prepared from grape seeds[109] as carbon source was recorded near 220 and 290nm (Figure 6A), which was caused by π-π * transition and n-π * transition caused by sp^2 aromatic structure, respectively.[110,111] The CQDs prepared by sweet corn[9] had an absorption peak at 260 nm, which belongs to the π-π* transition caused by C = C bonds and the n-π* transition caused by C = O bonds. The N-CQDs synthesized by Lu et al.[112] from watermelon juice had obvious absorption at 282nm and weaker than that at 355nm, which was attributed to the π - π * transition caused by C = C or C = N bonds and the n-π * transition of C = O bonds, respectively (Figure 6B).

3.2.2 | Photoluminescence

Effect of carbon source on photoluminescence

The composition of various biomass is different, which directly affects the fluorescence property of biomass carbon dots. The principal component of plants and their derivatives is sugar including cellulose, starch, maltose, and glucose.[113] The transition mode of n-π^* will occur due to the presence of C = O bond in sugar for the carbon dots from plants and their derivatives.[114] There are two transition modes of n-π^* and π-π^* in the generation of fluorescence for most biomass carbon dots. The rate constant of crossing the band gap to the triplet state is smaller during the π-π^* transition process than n-π^* transition, so the π-π^* transition is conducive to emit strong fluorescence. Therefore, the transition mode of n-π^* limits the improvement of the fluorescence property of biomass carbon dots to a certain extent. Benzene is common in the bark and fruit of plants, which is related to the color of flowers and fruits. The presence of benzene can increase the conjugated degree of the system, so it is easy to realize the π-π^* transition, thus enhancing the fluorescence of biomass carbon dots.[115] Because the conjugation effect can increase the molar absorbance coefficient of the biomass carbon dots, which is conducive to producing more excited molecules to achieve the effect of fluorescence enhancement.[116] Therefore, it is a breakthrough point to improve the fluorescence properties of biomass carbon dots by changing the transition mode and increasing the conjugation degree of the system. The principal component of animals and their derivatives mainly contains lipids and amino acids.[117] The existence of electron-withdrawing groups such as -COOH and -C = O in the lipids and amino acids is an crucial reason for the decrease in fluorescence of biomass carbon dots. But the amino groups in amino acids are electron donor groups, which will help enhance the fluorescence of biomass carbon dots from animals and their derivatives. The components of municipal waste are more complex and diverse. Some heteroatoms may be introduced inadvertently in biomass carbon dots to achieve self-doping to change the internal structure and thus change the fluorescence property for carbon dots from municipal waste.[118,119]

Effects of structure and composition on photoluminescence

Size : Carbon dots with different sizes have different energy levels, and their responses to light are different. Carbon dots with larger size have higher sensitivity to light response at longer wavelength, while carbon dots with smaller size are more sensitive to shorter wavelength. Blue and green emitting CQDs were prepared using beetroot extract as carbon source. The maximum emission positions were 450 nm (blue light) and 520 nm (green light), respectively.[75] Therefore, different sizes of carbon dots present different fluorescence effects. Generally, the narrower the size distribution of carbon dots means the better the fluorescence performance. Otherwise, too many intermediate energy levels will be formed in the forbidden band, making ineffective recombination increase.

Crystallinity : Crystallinity is an important parameter to measure the structure of carbon dots. The crystallinity of carbon dots can be characterized by Raman spectroscopy. The higher the intensity ratio of G peak (1600 cm^{-1}) to D peak (1360 cm^{-1}), the higher the crystallinity of carbon dots. GQDs can exhibit higher crystallinity and possess fewer atomic layers than CQDs. In general, higher crystallinity indicates that the carbon dots have a relatively complete sp^2 conjugated structure, which means higher fluorescence intensity and fluorescence QY.[120]

Heteroatoms doping : Heteroatoms can be doped into the internal structure of carbon dots, which will affect the fluorescence properties of carbon dots by changing their electronic characteristics, defect degree, and band structure. Heteroatom doping is one of the important means to improve the fluorescence properties of carbon dots, It has been reported in many literature that the fluorescence property of carbon dots can be improved by this method. However, the influence of types of heteroatoms on the fluorescence performance of carbon dots is also different. The lone pair of electrons from non-metal atoms can be effectively paired with carbon, while the introduction of metal atoms can change the energy level structure of carbon dots. The difference in the pairing mode and energy level structure will lead to the variation of the fluorescence intensity of the carbon dots.

Unlike carbon dots synthesized by small molecules, biomass carbon dots are rich in composition. To a certain extent, self-doping can be realized without deliberately introducing some heteroatoms, which is also the advantage of the biomass carbon dots. Liu et al.[118] synthesized nitrogen self-doped carbon dots by microwave-assisted hydrothermal method using peanut shell, cotton stalk, and soymeal as biomass carbon source without any additives. Similarly, the self-doping effect can be achieved using pork rib bones as raw materials to prepare carbon dots.[119] In addition, heteroatoms doping can improve the ordering and crystallinity of carbon dots, thereby improving fluorescence performance.[119,121]

Functional group : Functional groups are another important factor affecting the optical properties of carbon dots. The existence of oxygen-containing functional groups makes the defect states were formed on the surface of carbon dots, which result in different energy levels.[122] It has been reported that the surface defects of carbon dots caused by oxidation may lead to defect energy levels.

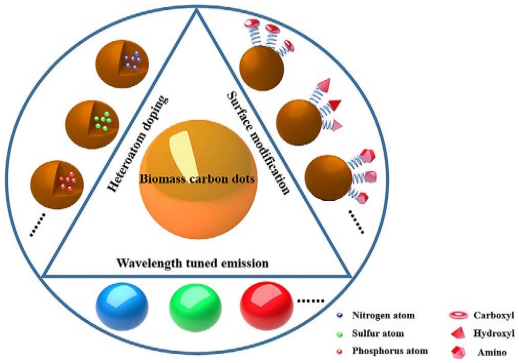

FIGURE 7 The photoluminescence adjustment of biomass carbon dots

The defect energy level will trap electrons or holes when the defect energy level is lower than the exciton energy level. The exciton will emit the surface defect state fluorescence through the defect state recombination.[123] In addition, nitrogen-containing functional groups can also affect the surface state of carbon dots. Due to electron withdrawing functional groups such as carboxyl groups on the surface of carbon dots without any passivated, the non-radiation-hole rearrangement centers are formed in the carbon dots, and the electron cloud density is reduced, which lead to lower fluorescence intensity.[124] Therefore, molecules with amino groups were often used for surface modification to convert the carboxyl groups into -CONHR or -CNHR to increase the luminance of carbon dots.[125] In general, electron-donating groups such as -OH, -OR, -CN, $-NH_2$, $-NR_2$ will increase the fluorescence intensity, while electron-withdrawing groups such as -COOH, $-NO_2$, -C = O, and halogen will weaken and even quench the fluorescence intensity.

Adjustment of photoluminescence

To make biomass carbon dots better used in the fields of bioimaging and analysis detection, it is particularly important to adjust the photoluminescence of them. The photoluminescence adjustment of biomass carbon dots was shown in Figure 7.

Wavelength tuned emission : Quantum dots can emit fluorescence with different colors by adjusting the wavelength position. The frequency will increase as the obstruction decreases when the wavelength is shorter. As a result, the energy of the photon is higher and the fluorescence of different colors is emitted. The emission wavelengths are in the range of 380–450, 450–475, 476–495, 495–570, 570–590, 590–620, and 620–750 nm, which belong to purple light, blue light, cyan light, green light, yellow light, orange light, and red light, respectively.

Four different CQDs were prepared by thermal calcination method using sorghum, pennisetum glaucum, rice, and wheat as carbon sources at the same time.[126] The emission wavelengths were 431, 421, 433 and 430 nm when the CQDs was excited at 310 nm, respectively. The defect state of CQDs was studied through the Gaussian analysis of the emission spectrum for better application in sensing. Among them, the QY of CQDs prepared with pennisetum glaucum was the highest (up to 33%), and that of CQDs from wheat was the lowest (reach to 16%), indicating that the carbon source is a crucial factor affecting the QY under the same treatment conditions. At present, many biomass carbon dots can emit different single color fluorescence, blue fluorescence of carbon dots can be seen by the naked eye, which were prepared from waste tea leaves and peanut shells,[127] silk fibroin,[41] crab shell,[12] anthracite coal,[55] green fluorescence of that from petroleum asphalt,[65,128] yellow fluorescence of that from coal,[17] red fluorescence of that from green tea,[22] orange fluorescence of that from durian,[129] and so on.

However, multi-color emission can be achieved from only one biomass by adjusting the process according to several reports. Using sugar beet extract[75] as a carbon source, the blue and green fluorescence CQDs were prepared through its hydrothermal and orthophosphoric acid treatment, respectively. Ye et al.[16] synthesized CQDs emitting fluorescence from green to orange-red using anthracite as carbon source. One method was to separate CQDs with different sizes by cross-flow ultrafiltration, and the other was that biomass carbon dots of different sizes were directly synthesized by controlling the reaction temperature (Figure 8A and 8B). Therefore, the size and band gap of biomass carbon dots can be adjusted by these methods, facilitating the broad application of it in different fields. Bhamore et al.[130] could synthesize the carbon dots emitting blue, green, and yellow fluorescence through different chemical oxidation methods, and the QY of carbon dots could reach 5.7%, 7.9%, and 5.2%, respectively.

Quantum yield and its adjustment : In addition to the green and non-toxic for raw materials themselves, the preparation of carbon dots from biomass can even achieve the purpose of reuse of waste and greatly reduce the synthesis cost. However, its fluorescence intensity and QY are not ideal compared with carbon dots prepared by small molecules, which may be due to the complex composition of biomass materials and the difficulty of separate extraction of certain substances, leading to the impurities that are not conducive to the performance of carbon dots may be introduced in the preparation process. Therefore, heteroatom doping and surface modification were carried out by many researchers to improve the performance of carbon dots and achieved relatively good results.

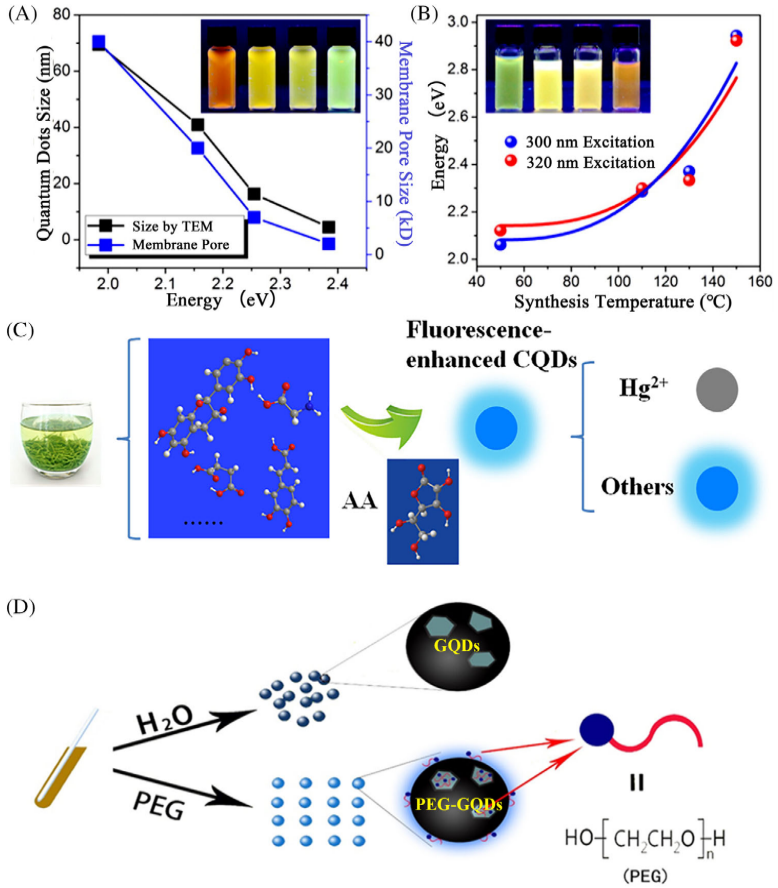

FIGURE 8 A, Relationship between the optical bandgap and GQDs size in the ultrafiltration (Inset: solution of GQDs under 365 nm excitation UV lamp), (B) Relationship between the optical bandgap and synthesis temperature at 300 and 320 nm excitation wavelength (Inset: solution of GQDs under 365 nm excitation UV lamp), (C) Illustration of the formation process of (AA)-enhanced CQDs from green teas by hydrothermal treatment and their multi-function application and (D) Schematic illustration of the function of PEG for GQDs. Reproduced with permission.[16] Copyright 2015, American Chemical Society. Reproduced with permission.[143] Copyright 2019, Elsevier. Reproduced with permission.[30] Copyright 2020, American Chemical Society

Heteroatom doping is the introduction of a small amount of non-metallic elements or metal ions into the lattice of carbon dots to form doping or defect energy levels, thus improving the optical properties of carbon dots. The introduction of heteroatoms may make the intrinsic quantum dots that do not emit light at high temperatures have high a luminous efficiency. The band gap can be effectively adjusted when the internal structure of the carbon dots is doped with heteroatoms, thus changing the transition mode of electrons, so that the adjustment of the carbon dots fluorescence performance can be realized. Markovic et al.[131] prepared F-CQDs and Cl-CQDs by one-step hydrothermal route, whose band gaps were increased by 2.0 and 1.7 eV respectively compared with the undoped CQDs. The QY of the P-doped carbon dots obtained by Zhou et al.[132] was more than eight times higher than that of undoped carbon dots, which was due to the existence of sp^2 clusters in the P-doped carbon dots increases the energy gap. Liu et al.[133] systematically studied the effect of nitrogen doping amount on carbon dots. The results showed that nitrogen doped carbon dots could produce intermediate energy levels, and the red shift phenomenon appeared with the increase of nitrogen doping amount.

Typical heteroatoms include nitrogen (N), sulfur (S), phosphorus (P), etc. It was found that N-doping can significantly enhance the photoluminescence. N-CQDs with

good dispersion and stability was prepared by hydrothermal method using orange juice and ethylenediamine as carbon source and nitrogen source respectively.[134] Photoluminescence spectra showed that the fluorescence intensity of N-CQDs increased with the increase of nitrogen doping amount. The QY was as high as 31.7%. However, the QY of undoped carbon dots prepared by the same carbon source and method was 26%.[135] N,S-CQDs with bright green fluorescent were prepared using palm shell powder and metafluoric acid as raw materials, which could be used as fluorescent probes for nitrophenol and realizing the sensitivity detection of NP, DNP, TNP.[136] The blue-green fluorescent N, S, P-CQDs prepared by hydrothermal method using natural foxtail millet as the carbon source possess high QY (~21.2%) and long fluorescence lifetime (~2.05 ns), realizing the sensitive detection of iron ions.[137] Nitrogen doping plays a very critical role in improving the properties of quantum dots. Many researchers have introduced nitrogen more or less into biomass carbon dots to improve the properties.[138–142]

The quantum effect of carbon dots with different sizes is caused by different emission traps on the surface. Effective surface passivation is necessary for carbon dots to emit strong photoluminescence. The photoluminescence properties that meet the requirements can be obtained by different surface passivation. The QY of carbon dots without modification is usually not high. To meet the needs of specific applications, the surface passivation and functionalization of biomass carbon dots are carried out through covalent binding, coordination, π-π interaction and so on.

Using green tea Maojian[143] as a carbon source, CQDs with ascorbic acid (AA) enhanced fluorescence performance were synthesized (Figure 8C). The QY of the CQDs could reach 12.79%, which is higher than that of the CQDs prepared by other methods or materials reported in the literature.[144–146] This may be due to the large variety and number of surface functional groups of AA-enhanced CQDs, such as carboxyl, hydroxyl, and amino groups. The CQDs could effectively detect Hg^{2+} in complex samples such as wastewater, tea, and rice. Our research group has been engaged in the research and application of biomass-based nanomaterials in recent years. Poly(ethylene glycol) passivated graphene quantum dots (PEG-GQDs) with bright blue fluorescence were synthesized by the hydrothermal treatment of cane molasses. The QY of PEG-GQDs is increased by more than 200% compared with GQDs without PEG passivation. This was due to the fact that PEG is a long-chain polymer containing abundant hydroxyl groups, which could achieve encapsulate for the inner GQDs (Figure 8D).[30] Using neem leaves[147] as carbon source, the fluorescence intensity of GQDs modified by amino was higher and more stable than that of unmodified GQDs. High fluorescence GQDs were prepared from coffee grounds[148] by functionalization with polyethyleneimine (PEI). The QY of PEI-GQDs was up to 24%, while that of GQDs without modification was only 8%. Similarly, the QY of GQDs was also increased by 50% after modified with amine by using rice[87] as carbon source.

4 | LUMINESCENCE MECHANISM OF BIOMASS CARBON DOTS

In the past decade, the preparation and application of carbon dots have made significant progress. The luminescence mechanism of carbon dots has been discussed by more and more researchers. However, due to the diversity of methods for preparing carbon dots, the size, chemical structure, and color of the prepared carbon dots are different, so the proposed luminescence mechanism is still controversy. Based on the current research results, the luminescence of carbon dots mainly involves the three following possible mechanisms, the defect-induced luminescence mechanism of conjugated π structure, quantum confinement effect mechanism, and fluorescent small molecules or fluorophores. Among these mechanisms, the first two were band gap luminescence, and the last one belongs to molecular luminescence. A diagram of the three specific luminescence mechanism was shown in Figure 9.

4.1 | Defect-induced luminescence mechanism

The defect-induced luminescence means that defects exist in most carbon dots, where electron and hole pairs are easy to form, the continuous band splits into different energy level structures, and different defects bring more sub-levels. With the continuous deepening of the research, the surface defect was the position that has no perfect sp^2 domain.[149,150] Surface defects can be divided into purity defects and impurity defects according to the amount of impurities. Among them, impurity defects will cause some fluorescence loss and reduce the QY. It was found that the purity defects in carbon dots generally include topological defects, oxygen-containing defects and nitrogen-containing defects. Topological defects are hexagonal lattice damage defects in carbon dots, while oxygen-containing and nitrogen-containing defects are active surface groups such as hydroxyl, carboxyl, and amino groups on the surface of carbon dots. At present, there are not many reports on the luminescence mechanism of biomass carbon dots, but it is similar to that of carbon dots obtained by small molecules. The content of functional groups on the surface of N-CQDs with high QY directly affected on photoluminescence.[151] Similarly,

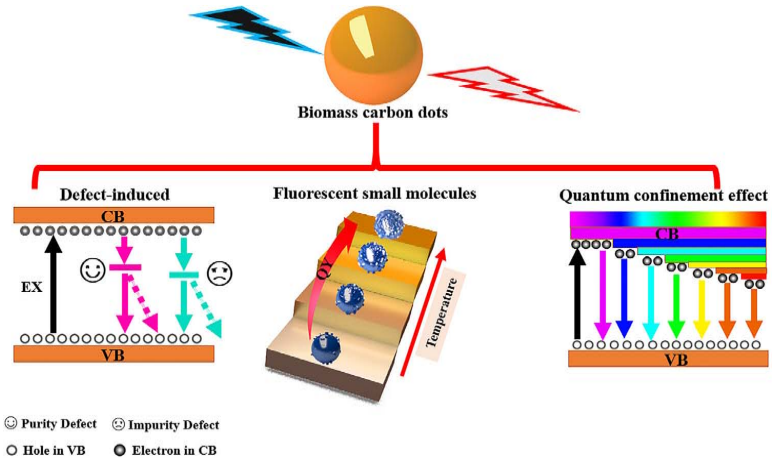

FIGURE 9 Three luminescence mechanisms of biomass carbon dots

Wu et al.[152] synthesized N-CQDs were more likely to be attributed to surface defects. One of luminescence mechanisms of the adjustable-size carbon dots synthesized using coal[153] as carbon source was caused by surface defects. Liu et al.[154] obtained CQDs and the luminescence mechanism was explained as the defect state luminescence caused by the active groups including –COOH, $–NH_2$, and C–N on the surface. This mechanism could achieve the effect of fine-tuning the fluorescent color of CQDs. The luminescence mechanism of S,N-CQDs synthesized from waste foam was also explained as the band gap luminescence caused by surface states.[155] The CQDs derived from Tofu wastewater could emit blue and green fluorescence due to the different surface functional groups.[156]

4.2 | Quantum confinement effect mechanism

As mentioned above, electrons and holes can be indirectly recombined due to the existence of defect centers, which cannot explain the fluorescence properties of carbon dots with few or almost no defects on the surface. The reason is that the surface of these carbon dots does not have so many chemical groups to form oxygen-containing or nitrogen-containing defects so that electrons and holes are indirectly recombined under the induction of the defect center. However, due to its size-limited conjugated π structure, the valence band and conduction band can be separated from the non-local molecular orbit of carbon dots, which lead to the electrons in the conduction band jumping to the holes in the valence band without the induction of the defect centers, so that the electrons and holes are directly combined, resulting in band gap fluorescence. The mechanism of direct recombination of electrons and holes is based on the fact that there are two hybrid carbon atoms sp^2 and sp^3 in these carbon dots, in which the particle size of sp^2 hybrid carbon atom is smaller, so it can diffuse into the sp^2 hybrid carbon skeleton. Since the electrons in the π and π^* energy levels of the sp^2 hybridization are affected by the σ and σ^* states of the sp^3 hybridization, the electron pairs from sp^2 hybrid carbon atoms will undergo transitions to produce fluorescence. When the particle size of the quantum dots was smaller than the Bohr radius of the exciton, the average free path of the electron is limited to a very small range, and the kinetic energy of the exciton increases, which leads to the increase of the effective band gap of the quantum dots and the blue shift. According to the current research results, the quantum confinement effect luminescence mechanism is widely more accepted than the other two luminescence mechanisms. Liu et al.[154] could realize the multi-color emission of CQDs from blue to red by adjusting the electronic transition caused by the quantum confinement effect. Wen et al.[157] obtained blue and green fluorescence CQDs separated by gel column chromatography, which were verified as the existence of fluorescence characteristics of the quantum confinement effect. Kim et al.[158] obtained GQDs with different sizes by using dialysis bags of different specifications. It was found that the shape and position of fluorescence emission peaks were related to the size of CQDs. A red shift of the fluorescence emission peak occurred with the increase of GQDs diameter to 17 nm, which was consistent with the law of fluorescence emission caused by the quantum confinement effect. Zhu et al.[159] synthesized a variety of GQDs with different sizes, which was related to the internal energy

state of GQDs, and the energy level compensation between the internal energy state and the edge energy state determines the optical properties of GQDs. Zhu et al.[160] confirmed the luminescence mechanism by density functional theory (DFT) calculations that the fluorescence of the obtained N-CQDs is mainly derived from the emission induced by the π-π^* transition. Accordingly, many reports on the luminescence mechanism of carbon dots were belonged to quantum confinement effect.[150,161–163]

4.3 | Fluorescent small molecules

The luminescence mechanism of fluorescent small molecules is different from the first two band gap luminescence mechanisms. In addition to defects in carbon dots, there is also a fluorescent small molecule or fluorophore, which can also emit fluorescence. These small molecules are similar to dye molecules and can be bonded to the surface of carbon dots or embedded in them. This fluorescence mechanism claims that the reason of the fluorescence of carbon dots is due to the different production of fluorophores and carbon nucleus at different temperatures, the number of which is closely related to the fluorescence properties of carbon dots. In other words, within a certain temperature range, the higher temperature will produce more fluorophores, resulting in higher QY. This luminescence mechanism of fluorescent small molecules is slightly less accepted than the first two. Shi et al.[164] synthesized molecular state luminescence CQDs with citrazine-like fluorophores by hydrothermal method. Fang et al.[165] systematically studied the photoluminescence properties of the synthesized CQDs. The results showed that the property was determined by the synergistic effect of the luminescent pyridine derivatives. Li et al.[70,84] synthesized near infrared (NIR)-light emitting fluorescent CQDs derived from spinach, the research results showed that the porphyrin in the chlorophyll from spinach had a molecular state at 120°C, but the absorption peak and PL emission peak of porphyrin disappeared when the temperature is increased to 180°C, which indicated the structure has a molecular state at 120°C. Similarly, the photoluminescence behavior of different color carbon dots prepared from tomato,[166] mango,[167] lemon juice,[7] pumpkin,[168] and waste kitchen chimney oil[67] was also related to the molecular state luminescence mechanism.

5 | APPLICATION OF BIOMASS CARBON DOTS IN SENSING

Biomass carbon dots can realize its value in analysis and sensing due to excellent fluorescence performance. They have many functional groups on the surface compared with non-biomass carbon dots, some substances including metal ions and non-metal molecules can interact with these groups to change their fluorescence properties. Based on the quenching mechanism, the quantitative analysis of various target detection can be achieved.

5.1 | Sensing of metal ions

Iron (Fe) is an indispensable element for hemoglobin. Iron deficiency will reduce hemoglobin synthesis and suffering from anemia for the human body. However, excessive iron intake will cause significant damage to cellular components, leading to tissue inflammation and multiple organ fibrosis. Similarly, endocrine disorders can be caused when copper (Cu) intake is insufficient, but excessive intake may cause poisoning, including acute copper poisoning, hepatolenticular degeneration, intrahepatic cholestasis in children, and so on. Similarly, excessive other metal ions, especially heavy metal ions, cause varying degrees of harm to organisms and the environment. Therefore, it is very significant to develop a convenient method to realize the quantitative detection of metal ions.

At present, more and more researchers have applied the synthesized biomass carbon dots to the detection of metal ions. The carbon dots prepared using poplar leaves,[169] lemon juice,[6] pear juice,[170] corncob,[171] and alkali lignin[139] as carbon sources could be used to detect iron ions. As more and more reports on the detection of iron ions by biomass carbon dots, researchers were also constantly striving to achieve continuous breakthroughs of the lowest of detection (LOD). Pramanik et al.[100] synthesized carbon dots from aegle marmelos leaves through a simple hydrothermal carbonization process, which was applied to the detection of iron ions. The LOD and linear detection range were 0.12 μM and 0–20 μM, respectively. The GQDs based on ligninsulfonate[172] had good sensitivity and selectivity to Fe^{3+} (Figure 10A and 10B), the linear range was 0.005–500 μM and the LOD was as low as 0.5 nM. The practical application of the probe in the determination of Fe^{3+} in lake water samples was further explored. Some biomass carbon dots had two different linear ranges for iron ions detection. For example, the blue fluorescent N-CQDs synthesized by the hydrothermal method with red lentils[173] had good selectivity to Fe^{3+} compared to other metal ions, the linear ranges for iron ion detection of 2–20 μM and 300–1000 μM (Figure 10C and 10D), the LOD could reach 0.1 μM. Even if the same biomass was used as carbon source, the sensitivity of biomass carbon dots prepared by different processes might be different. For example, Yuan et al.[98] prepared CQDs from tar by pyrolysis, its

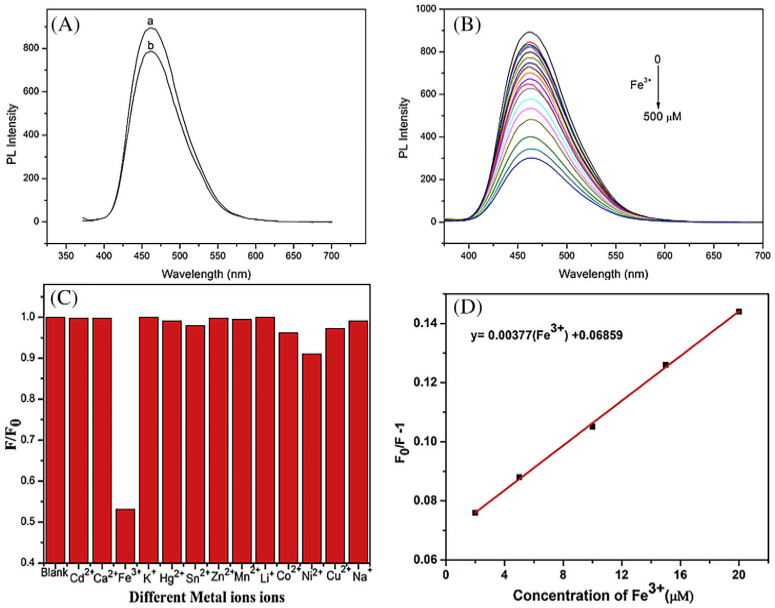

FIGURE 10 A, PL emission spectra of SL/GQDs from ligninsulfonate dispersion in the absence (curve a) and presence (curve b) of 50 μM Fe^{3+} ions, (B) PL emission spectra of SL/GQDs from ligninsulfonate dispersion in the presence of increasing Fe^{3+} concentrations (0–500 μM), (C) Change in relative fluorescence intensity of N-CQDs from red lentils at excitation wavelength 365 nm on addition of different metal ions and (D) Linear plot of $F_0/F - 1$ versus Fe^{3+} in the range 2–20 μM for N-CQDs from red lentils. Reproduced with permission.[172] Copyright 2016, Elsevier. Reproduced with permission.[173] Copyright 2019, Elsevier

QY could reach 53%, the linear detection range and LOD for iron ions were 0–100 μM and 0.22 μM, respectively. Deng et al.[141] also used tar as carbon source and ethylenediamine as nitrogen source to obtain N-CQDs with a QY of only 26.1%. Although the QY of synthesized CQDs was not as high as that of CQDs synthesized by Yuan et al.,[98] the N-CQDs indeed have better performance than undoped CQDs. And its linear range and LOD for the detection of Fe^{3+} were 0.06–1400 μM and 0.06 μM, respectively, which showed higher sensitivity and wider detection linear range than that of the CQDs synthesized by Yuan et al.[98]

The reports on detecting other metal ions by biomass carbon dots were slightly less compared with iron ions, which provide researchers with more possibilities and greater opportunities for breakthroughs. Excessive mercury ions may cause damage to the human central nervous system, and even death in severe cases. Currently, biomass carbon dots were also used for detecting mercury ions. CQDs with good biocompatibility were prepared by hydrothermal method using ginkgo leaves[174] as the precursor and applied to the detection of Hg^{2+}. The sensing system had a good linear relationship in the range of 0.5–20 μM, its detection limit was 12.4 nM. And the monitoring of Hg^{2+} in lake water and serum samples was realized. In addition, the carbon dots from green tea,[143] apple juice,[5] hair,[13] and prosopis juliflora leaves[175] could also achieve the detection of Hg^{2+}. Besides, biomass carbon dots could also apply to detecting other different metal ions such as Cu^{2+}, Ag^{+}, Cr^{6+}, Cr^{3+}, As^{3+}, and Co^{2+} and their LOD and related linear detection ranges were shown in Table 2.

5.2 | Sensing of non-metal molecules

In addition to metal ions, biomass carbon dots can also be used to detect some non-metallic molecules. The most typical one is the detection of H_2O_2, which could be achieved by biomass carbon dots from mustard seeds,[176] azadirachta Indica leaves,[177] salep[107], and alkali lignin.[102] S,N-GQDs was obtained from alkali lignin[102] by fractionation, and the LOD to H_2O_2 was as low as 0.13 nM. Density functional theory (DFT) showed that the sulfoxide group in the middle defect of S,N-GQDs was the binding site of H_2O_2. CQDs was obtained by simple hydrothermal treatment with salep as carbon source, and then embedding them with synthetic silver[107]

TABLE 2 Summary of biomass carbon dots applied in sensing

Carbon source	Analyte	Linear range	LOD	pH of system	Mechanism	Ref
Mangifera leaves	Fe^{2+}	100–1000 ppm	0.62 ppm	7	Inner filter effect	[190]
Magnolia flower	Fe^{3+}	0.2–1 μM	0.073 μM	6	Static quenching	[182]
Luffa sponge	Cr^{6+}	0–0.4 μg/L	/	/	Static quenching	[183]
poplar leaves	Fe^{3+}	0–2.5 μM	/	4-10	Static quenching	[169]
Ginkgo leaves	Hg^{2+}	0.5–20 μM	12.4 nM	7	/	[174]
Pear juice	Fe^{3+}	0–50 μM	2.28 μM	/	Forming complex	[170]
Green tea	Hg^{2+}	0.2–60 μM	6.32 nM	/	/	[143]
Purple perilla	Ag^{+}	0.5–10 /10–3000 nM	1.4 nM	7	Static quenching	[181]
Phosphorus	Co^{2+}	1.7–12/28-141 μM	29.4 nM	3-12	Static quenching	[103]
Corncob	Fe^{3+}	0–321 μM	0.75 μM	10	/	[171]
Eleusine coracana	Cu^{2+}	0–100 nM	10 nM	/	Inner filter effect	[91]
Aminated alkali lignin	Fe^{3+}	100 nM–1 mM	8 nM	7	/	[138]
Red lentils	Fe^{3+}	2–20 / 300–1000 μM	0.1 μM	7	Static and dynamic quenching	[173]
Prosopis juliflora leaves	Hg^{2+}	2.5–22.5/ 5–500 ng /mL	6.3 nM	8	Electron transfer	[175]
Pinellia ternata	Cr^{6+}	0–200 μM	15 nM	7	Non-radiative transition	[213]
Watermelon juice	Fe^{3+}	0–300 μM	0.16 μM	3-9	Interaction	[112]
	cysteine	0–250 μM	0.27 μM		Turn on	
Alkali lignin	Fe^{3+}	0–500μM	0.44 μM	1-11	Forming complex	[139]
Tuberose petals	Fe^{3+}	/	/	7	/	[214]
	Cu^{2+}	0–70 μM	200 nM			
Quince fruit	As^{3+}	0.1–2 μg/mL	0.02 μg/mL	5	/	[105]
Eleocharis dulcis	Fe^{3+}	50–350 μM	0.56 μM	7	Nonradiative recombination	[99]
Broccoli	Ag^{+}	0–600 μM	0.5 μM	7	Forming complex	[215]
Foxtail millet	Fe^{3+}	5–150 μM	0.046 μM	/	Forming complex	[137]
Tamarindus indica leaves	Hg^{2+}	0–0.1 μM	6 nM	7	non-radiative electron transfer	[216]
	glutathione	0–20 μM	1.7 μM		Turn on	
Aegle marmelos leaves	Fe^{3+}	0–20 μM	0.12 μM	7	PET	[100]
Jackfruit	Hg^{2+}	5–70 nM	8 nM	7	Non-radiative electron transfer	[101]
	Cr^{6+}	5–70 nM	10 nM		Interaction	
Orange juice	Hg^{2+}	0–32 μM	/	10	Forming complex	[134]
Lemon juice	Fe^{3+}	1–90 μM	2.5 μM	7	Static and dynamic quenching	[6]
Apple juice	Hg^{2+}	5.0–100.0 nM /1.0–50.0 μM	2.3 nM	7	Affinity	[5]
Bamboo leaves	Cu^{2+}	0.333–66.6 μM	115 nM	4	Forming complex	[95]
Citrus peels	Fe^{3+}	0.01–1.0 μM	3.0 nM	3	Inner filter effect	[191]
	tartrazine	0.6–23.5 μM	0.2 μM	7		
Magnolia flower	Fe^{3+}	0.2–1 μM	0.088 μM	6	Static quenching.	[182]

(Continues)

TABLE 2 (Continued)

Carbon source	Analyte	Linear range	LOD	pH of system	Mechanism	Ref
Sorghum	Cr^{3+}	1–14 μM	0.689 μM	7	Electron movement	[126]
Pearl millet			1.246 μM			
Rice			0.833 μM			
Wheat			0.746 μM			
Ligninsulfonate	Fe^{3+}	0.005–500 μM	0.5 nM	7	Forming complex	[172]
Rice husk	Fe^{3+}	0–0.1 mM	5.8 nM	7	Forming complex	[104]
Hair	Hg^{2+}	0–75 μM	0.01 μM	5	Static and dynamic quenching	[13]
Escherichia coli	Fe^{3+}	0.58 nM–100 μM	0.58 nM	/	/	[140]
Rice residue	Fe^{3+}	3.32–32.26 μM	0.7462 μM	4	Static quenching	[108]
	Tetracycline		0.3739 μM		/	
	Chlortetracycline		0.2791 μM			
	Terramycin		0.2367 μM			
Tar	Fe^{3+}	0.06–1400 μM	0.06 μM	4-5	Forming complex	[141]
Tar	Fe^{3+}	0–100 μM	0.22 μM	7.6	Energy transfer	[98]
Chocolate	Pb^{2+}	0.033–1.67 μM	12.7 nM	7	Electron transfer	[217]
Tulsi leaves	Cr^{6+}	1.6–50 μM	4.5 ppb	7	IFE	[192]
Bergamot	Fe^{3+}	0.025–100 μM	0.075 μM	7.4	Static quenching	[218]
	Hg^{2+}	0.01–100 μM	5.5 nM	7.0		
Lotus root	Hg^{2+}	0. 1–60 μM	18.7 nM	7.0	Static quenching	[219]
Lemon peel	Cr^{6+}	2.5–50 μM	73 nM	7	Non-radiative recombination	[220]
Phyllanthus acidus	Fe^{3+}	2–25 μM	0.9 μM	7	Radiative transition	[221]
Prunus avium fruit	Fe^{3+}	0–100 μM	0.96 μM	7	Non-radiative electron or energy transfer	[222]
Cherry Tomatoes	Trifluralin	0.050–200 μM	0.5 nM	2–11	Static quenching	[96]
Algae	Nonylphenol	0.01–1.2 μM	0.1 μM	/	Interaction	[223]
Sweet corn	S^{2-}	5–100 nM	8 nM	7	Non-radiative electron transfer	[9]
Mango peels	Mesotrione	15–3000 nM	4.7 nM	8	FRET	[187]
Sucrose	VB_{12}	2–31 μM	3 nM	3-12	Inner filter effect	[103]
Mustard seeds	H_2O_2	0.02–0.2 mM	0.015 mM	4	Catalytic	[176]
	Ascorbic acid	10–70 μM	3.26 μM			
cornstalk	Candida albicans	$2.60 * 10^5$–$1.99 * 10^8$ cfu/mL	1124 cfu/mL	7.4	Specifically combine	[142]
Azadirachta indica Leaves	H_2O_2	0.1–0.5 mmol/L	0.035 mmol/L	4	Catalytic	[177]
	Ascorbic Acid	5–40 μM	1.773 μM			
Palm shell	phenol	0.2–0.40 μM	0.079 μM	6–8	FRET	[136]
	p-Chlorophenol	0.5–85 μM	0.165 μM			
	monocrotophos	0.20–40 μM	0.082 μM			
Beet	Amoxicillin	0–400 μM	0.475 μM	6	Hydrogen bonding	[224]
Orange juice	promethazine hydrochloride	2.0–250 μM	0.5 μM	7	Molecular imprinting	[225]
Salep	H_2O_2	0.2–27 μM	80 nM	7	Catalytic	[107]
Green tea	catechins	0.01–30 μM	0.005 μM	8.4	Catalytic and electron transfer	[226]

(Continues)

TABLE 2 (Continued)

Carbon source	Analyte	Linear range	LOD	pH of system	Mechanism	Ref
Alkali lignin	H_2O_2	0–150 nM	0.13 nM	9.18	Intramolecular charge transfer	[102]
Whey	selenite	10–50 μg/ L	0.035 ppb	/	/	[88]
Cigarette filters	Sudan I	2.40–104.0 μM	0.95 μM	6.09	Energy transfer	[97]
Coal	phenol	0–40 μM	0.076 μM	7	Hydrogen bonds	[178]
Aloe	tartrazine	0.2–32.50 μM	73 nM	6.0	Static quenching	[227]
Tomato juice	carcidoembryonic antigen	5.65 nM–50 μM	1.88 nM	7.4	PET	[228]

nanoparticles (AgNPs). The final AgNPs/CQDs could be applied to the detection of H_2O_2. The electrochemical results showed that the material had a good catalytic performance for H_2O_2 reduction. The linear range and LOD of H_2O_2 were 0.2–27.0 μM and 80 nM, respectively. The detection of H_2O_2 in bovine serum was realized. The CQDS prepared by one-step hydrothermal treatment of mustard seeds[176] showed similar peroxidase activity. It could catalyze the oxidation of the chromogenic substrate 3,3',5,5'-tetramethylbenzidine (TMB) to form a blue reaction mixture in the presence of H_2O_2. Based on this, the detection of H_2O_2 could be realized. The linear range and LOD were 0.02–0.2 mM and 0.015 mM, respectively. Coincidentally, the CQDs obtained by Yadav et al.[177] through hydrothermal treatment of leaf extracts of neem were applied to the detection of H_2O_2 based on the almost identical mechanism. Selenite, Sudan I and phenol could be detected by biomass carbon dots from whey,[88] cigarette filters,[97] and coal,[178] respectively. The specific detection results and other detectable targets were shown in Table 2. Three kinds of tetracycline could be visually distinguished through carbon dots from tobacco.[179]

5.3 | Quenching mechanism

The reason why biomass carbon dots can realize the detection of metal ions or non-metal molecules is that the fluorescence properties of carbon dots respond to these additions. Most of the detected targets can quench the fluorescence of the carbon dots, which is a physical or chemical interaction between the carbon dots and the solvent or solute molecule, leading to the decrease of fluorescence intensity. Various detection methods may be due to different quenching mechanisms including static quenching, dynamic quenching, Förster resonance energy transfer (FRET), photo-induced electron transfer (PET) and internal filtration effect (IFE), etc. A more vivid quenching mechanism was shown in Figure 11.

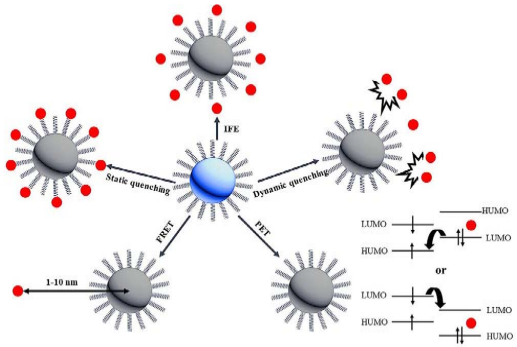

FIGURE 11 Common quenching mechanisms of biomass carbon dots

5.3.1 | Static quenching

In this paper, static quenching refers to the formation of non-luminescent ground state complexes between the biomass carbon dots and the quencher. The quenching is a process that competes with the luminescence to shorten the lifetime of excited states of luminescent molecules. However, static quenching is the interaction between the quencher and the ground state molecules of the carbon dots. Thus, static quenching meets the following conditions: (1) The fluorescence lifetime of the carbon dots does not change after adding quencher. (2) The absorption spectrum of the carbon dots changes after adding quencher. (3) The quenching constant decreases with the temperature increases.[31,180] The mechanism of the quenching of CQDs by Ag^+ from purple perilla[181] (Figure 12A and 12B) has been verified to be static quenching based on these three judgments. Many other biomass carbon dots have also been reported based on the static quenching mechanism to realize the detection of targets, such as the carbon dots derived from magnolia flower,[182] luffa sponge,[183] poplar leaves,[169] and sucrose.[103]

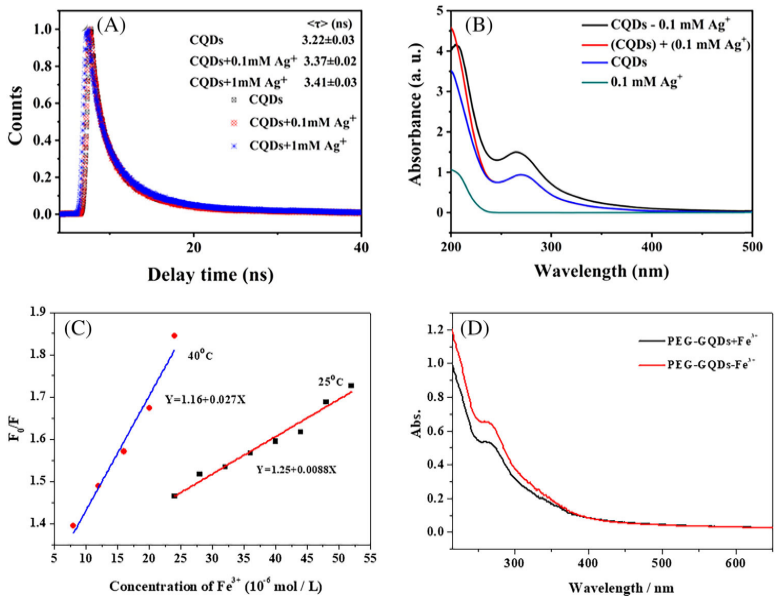

FIGURE 12 A, Fluorescence decay traces of CQDs from purple perillaand with addition of different concentration of Ag^+ solution, (B) UV–vis absorption spectra of CQDs from purple perilla(blue), Ag^+ (green), CQDs-Ag^+ system (black), and summed UV–vis absorption spectrum between CQDs and Ag^+ (red), respectively, (C) Stern–Volmer curve for fluorescence quenching of PEG-GQDs from cane molasses by Fe^{3+} at different temperatures and (D) the UV-vis absorption spectra of PEG-GQDs from cane molasses in the presence of Fe^{3+} (red curve) and the superposition of the UV-vis absorption spectra ofPEG-GQDs and Fe^{3+} solutions (black curve). Reproduced with permission.[181] Copyright 2019, Elsevier. Reproduced with permission.[30] Copyright 2020, American Chemical Society

5.3.2 | Dynamic quenching

Dynamic quenching means that the excited state molecules of the biomass carbon dots lose their excitation energy through the collision of the quencher molecules based on energy transfer or charge transfer and return to the ground state. It is the interaction between the quencher and the excited state molecules of the carbon dots. Dynamic quenching is linked to the diffusion coefficient, which promotes the movement of molecules with the increase of temperature. Thus, dynamic quenching meets the following conditions: (1) The presence of the quencher shortens the fluorescence lifetime of the carbon dots. (2) The absorption spectrum of the carbon dots does not change after adding quencher. (3) The quenching constant increases with the temperature increases.[31,180] The mechanism of the quenching of Fe^{3+} by GQDs from cane molasses[30] (Figure 12C and 12D) has also been confirmed based on these three judgments.

Thus, dynamic quenching and static quenching can be distinguished from fluorescence lifetime, quenching coefficient, and absorption spectrum. However, static quenching and dynamic quenching might co-occur in the same biomass carbon dots, such as the carbon dots from red lentils,[173] lemon juice,[6] and hair.[13]

5.3.3 | FRET quenching

Energy transfer includes radiated energy transfer and non-radiative energy transfer according to the different mechanism. Among them, non-radiative energy transfer can be divided into FRET through dipole-dipole coupling and exchange energy transfer through electron exchange. In contrast, the FRET mechanism is more common for biomass carbon dots. FRET quenching complies with the following conditions: (1) The emission spectrum of carbon dots overlaps with the absorption spectrum of the quencher. (2) The fluorescence lifetime of the carbon dots is shortened, that is, $\tau_0/\tau > 1$. (3) The distance between the carbon dots and the quencher is 1–10 nm.[184–186] Soni et al.[136] used palm shell waste as biomass carbon source to synthesize N,S-CQDs which could be applied to the detection of nitrophenol. Moreover, Sun et al.[187] prepared CQDs from mango peels which can be quenched by mesotrione. The carbon dots from apple seeds were applied

to the detection of 4-NP.[188] All of the above fluorescence quenching mechanism for detection can be attributed to FRET.

5.3.4 | PET quenching

PET quenching refers to the phenomenon that electrons undergo intramolecular or intermolecular transfer under the induction of light, usually from the donor to the excited state fluorophore. Therefore, carbon dots do not emit or emit very faint fluorescence before binding to the guest. PET quenching meets the following conditions: (1) Fluorescence lifetime of carbon dots decreased after adding quencher. (2) The LUMO and HOMO energy gap exists between carbon dots and quencher.[186] Pramanik et al.[100] synthesized CQDs using aegle marmelos leaves for the detection of Fe^{3+} and verified this quenching mechanism.

5.3.5 | IFE quenching

IFE quenching refers to the phenomenon that the excited light or emitted light of the carbon dots is absorbed by certain substance in the solution. It can cause the deviation of the linear relationship between the fluorescence intensity of carbon dots and the concentration of detection of target, and even distort the spectrum shape. IFE quenching meets the following conditions: (1) The overlap of the emission and absorption spectra of biomass carbon dots. (2) The absorption peak does not change after adding quencher. (3) Fluorescence lifetime does not change after adding quencher. (4) The Parker equation can further verify the IFE quenching.[186,189] It has also been mentioned from many reports, such as the carbon dots from mangifera leaves,[190] eleusine coracana,[91] citrus peels,[191] tulsi leaves,[192] and sucrose.[103]

6 | CONCLUSION AND OUTLOOK

In this review, we introduce in detail the carbon dots synthesized from different biomass carbon sources, which were divided into plants and their derivatives, animals, and their derivatives and municipal waste. Plants and their derivatives accounted for a larger proportion than the other two categories. The synthesis methods of biomass carbon dots are mainly hydrothermal and solvothermal methods. The morphology can be characterized by TEM, HRTEM, and AFM, and the composition and structure information can be obtained by XRD, FI-IR, and XPS, which are the most basic characterization methods for analyzing biomass carbon dots. Moreover, the regulation of photoluminescence and three common luminescence mechanisms for biomass carbon dots were described in detail. Finally, the biomass carbon dots applied to the detection of metal ions and non-metal molecules based on the quenching mechanism, including dynamic quenching, static quenching, FRET, PET, and IFE were illustrated.

Since the initial discovery of carbon quantum dots in 2004, it has always attracted the attention of researchers. In recent years, an upsurge has been set off in the preparation of carbon dots using biomass as carbon source. Biomass carbon dots showed many advantages including excellent fluorescence properties, good biocompatibility, low toxicity, and easy chemical modification for the application in detection. Biomass carbon dots can be used to detect tissue samples and the diagnosis of related diseases, which provide a new method for biological research. Biomass carbon dots combined with veterinary drug molecules added to the feed can be used to study the metabolic process of drug molecules in animals, so as to provide the basis for clinical medication. Food safety has always been a topic of concern to people, and health is an eternal pursuit. Therefore, the application of biomass carbon dots for the detection of pigments, additives, and pesticides will have a relatively broad prospect. With the rapid development of analytical chemistry, the trace analysis of heavy metal ions has become a research hotspot in the future. Biomass carbon dots have realized the detection of a variety of metal ions at present. Hence, biomass carbon dots will make more contributions in biology, food safety and quantitative analysis.

However, some bottlenecks exist in the current research of biomass carbon dots. The synthesis of biomass carbon dots is still in the laboratory stage, which is far from industrial production with high yield. No rigorous and feasible experimental scheme to further clarify the relationship between the microstructure of carbon dots and fluorescence properties, so the luminescence mechanism of biomass carbon dots has not yet been clarified. In terms of detection application, the specificity of the detection target and the detection sensitivity are not particularly satisfactory. There are very few reports on the multi-component simultaneous detection, which needs further research and exploration. With the development and in-depth research of biomass carbon dots, the above problems will be solved properly. Biomass carbon dots will serve people's lives as promising materials.

ACKNOWLEDGMENTS

This work was supported in part by the National Natural Science Foundation of China (No. 51564009), the Natural Science Foundation of Guangxi province

(No. 2018JJA160029) and the Foundation of Key Lab New Processing Technology for Nonferrous Metals & Materials Ministry of Education (No. 20AA-17).

ORCID

Aimiao Qin https://orcid.org/0000-0003-0834-0555

REFERENCES

1. Z. T. Fan, S. H. Li, F. L. Yuan, L. Z. Fan, *RSC Adv.* **2015**, *5*, 19773.
2. P. Zheng, N. Q. Wu, *Chem Asian J.* **2017**, *12*, 2343.
3. Y. Du, S. J. Guo, *Nanoscale*. **2016**, *8*, 2532.
4. M. T. Genc, G. Yanalak, G. Arslan, I. H. Patir, *Mater. Sci. Semicond. Process*. **2020**, *109*, 104945.
5. Y. Xu, C. J. Tang, H. Huang, C. Q. Sun, Y. K. Zhang, Q. F. Ye, A. J. Wang, *Chinese J. Anal. Chem.* **2014**, *42*, 1252.
6. T. K. Mondal, A. Gupta, B. K. Shaw, S. Mondal, U. K. Ghorai, S. K. Saha, *RSC Adv.* **2016**, *6*, 59927.
7. H. Ding, Y. Ji, J. S. Wei, Q. Y. Gao, Z. Y. Zhou, H. M. Xiong, *J. Mater. Chem. B*. **2017**, *5*, 5272.
8. M. Q. He, J. Zhang, H. Wang, Y. R. Kong, Y. M. Xiao, W. Xu, *Nanoscale Res. Lett.* **2018**, *13*, 175.
9. K. Rajendran, G. Rajendran, J. Kasthuri, K. Kathiravan, N. Rajendiran, *Chemistryselect.* **2019**, *4*, 13668.
10. S. J. Zhao, M. H. Lan, X. Y. Zhu, H. T. Xue, T. W. Ng, X. M. Meng, C. S. Lee, P. F. Wang, W. J. Zhang, *ACS Appl. Mater. Interfaces*. **2015**, *7*, 17054.
11. J. Wang, C. F. Wang, S. Chen, *Angew. Chem. Int. Ed.* **2012**, *51*, 9297.
12. Y. Y. Yao, G. Gedda, W. M. Girma, C. L. Yen, Y. C. Ling, J. Y. Chang, *ACS Appl. Mater. Interfaces*. **2017**, *9*, 13887.
13. Y. M. Guo, L. F. Zhang, F. P. Cao, Y. M. Leng, *Sci. Rep.* **2016**, *6*, 35795.
14. D. Sun, R. Ban, P. H. Zhang, G. H. Wu, J. R. Zhang, J. J. Zhu, *Carbon*. **2013**, *64*, 424.
15. R. C. Wang, J. T. Lu, Y. C. Lin, *J. Alloys Compd.* **2020**, *813*, 152201.
16. R. Q. Ye, Z. W. Peng, A. Metzger, J. Lin, J. K. Mann, K. W. Huang, C. S. Xiang, X. J. Fan, E. L. G. Samuel, L. B. Alemany, A. A. Marti, J. M. Tour, *ACS Appl. Mater. Interfaces*. **2015**, *7*, 7041.
17. Y. Q. Dong, J. P. Lin, Y. M. Chen, F. F. Fu, Y. W. Chi, G. N. Chen, *Nanoscale*. **2014**, *6*, 7410.
18. V. Wongso, N. S. Sambudi, S. Sufian, Isnaeni, *Biomass Conversion and Biorefinery*, https://doi.org/10.1007/s13399-020-00662-9.
19. N. Niu, Z. M. Ma, F. He, S. J. Li, J. Li, S. X. Liu, P. P. Yang, *Langmuir*. **2017**, *33*, 5786.
20. W. Du, X. Q. Xu, H. Hao, R. M. Liu, D. Zhang, F. Gao, Q. Y. Lu, *Sci China Chem*. **2015**, *58*, 863.
21. R. B. Qiang, S. R. Yang, K. M. Hou, J. Q. Wang, *New J. Chem.* **2019**, *43*, 10826.
22. N. Irmania, K. Dehvari, G. Gedda, P. J. Tseng, J. Y. Chang, *J. Biomed. Mater. Res. Part B Appl. Biomater.* **2020**, *108*, 1616.
23. D. Shukla, F. P. Pandey, P. Kumari, N. Basu, M. K. Tiwari, J. Lahiri, R. N. Kharwar, A. S. Parmar, *Chemistryselect.* **2019**, *4*, 4839.
24. X. Wang, P. Yang, Q. Feng, T. T. Meng, J. Wei, C. Y. Xu, J. Q. Han, *Polymers*. **2019**, *11*, 616.
25. I. Sargin, G. Yanalak, G. Arslan, I. H. Patir, *Int. J. Hydrogen Energy*. **2019**, *44*, 21781.
26. F. Temerov, A. Belyaev, B. Ankudze, T. T. Pakkanen, *J. Lumin.* **2019**, *206*, 403.
27. Z. Y. Ding, F. F. Li, J. L. Wen, X. L. Wang, R. C. Sun, *Green Chem.* **2018**, *20*, 1383.
28. A. Barati, M. Shamsipur, E. Arkan, L. Hosseinzadeh, H. Abdollahi, *Mater Sci Eng C Mater Biol Appl*. **2015**, *47*, 325.
29. P. Roy, A. P. Periasamy, C. Chuang, Y. R. Liou, Y. F. Chen, J. Joly, C. T. Liang, H. T. Chang, *New J. Chem.* **2014**, *38*, 4946.
30. Y. Lou, J. Y. Ji, A. M. Qin, L. Liao, Z. Y. Li, S. P. Chen, K. Y. Zhang, J. Ou, *ACS Omega*. **2020**, *5*, 6763.
31. W. Liu, H. P. Diao, H. H. Chang, H. J. Wang, T. T. Li, W. L. Wei, *Sens Actuators B Chem*. **2017**, *241*, 190.
32. Z. Y. Wang, H. Liao, H. Wu, B. B. Wang, H. D. Zhao, M. Q. Tan, *Anal. Methods*. **2015**, *7*, 8911.
33. A. Sachdev, P. Gopinath, *Analyst.* **2015**, *140*, 4260.
34. K. Bankoti, A. P. Rameshbabu, S. Datta, B. Das, A. Mitra, S. Dhara, *J. Mater. Chem. B*. **2017**, *5*, 6579.
35. B. De, N. Karak, *RSC Adv*. **2013**, *3*, 8286.
36. Y. Song, X. Yan, Z. H. Li, L. B. Qu, C. Z. Zhu, R. F. Ye, S. Q. Li, D. Du, Y. H. Lin, *J. Mater. Chem. B*. **2018**, *6*, 3181.
37. Y. K. Song, L. Cao, J. Q. Li, S. Cong, D. M. Li, Z. J. Bao, M. Q. Tan, *Food Funct.* **2019**, *10*, 3706.
38. A. Dehghani, S. M. Ardekani, M. Hassan, V. G. Gomes, *Carbon*. **2018**, *131*, 238.
39. S. J. He, M. J. Turnbull, Y. T. Nie, X. H. Sun, Z. F. Ding, *Surf Sci.* **2018**, *676*, 51.
40. M. Thakur, A. Mewada, S. Pandey, M. Bhori, K. Singh, M. Sharon, M. Sharon, *Mater Sci Eng C Mater Biol Appl*. **2016**, *67*, 468.
41. N. R. Ko, M. Nafiujjaman, K. Cherukula, S. J. Lee, S. J. Hong, H. N. Lim, C. H. Park, I. K. Park, Y. K. Lee, I. K. Kwon, *Part. Part. Syst. Charact.* **2018**, *35*, 1700300.
42. J. B. Essner, C. H. Laber, S. Ravula, L. Polo-Parada, G. A. Baker, *Green Chem.* **2016**, *18*, 243.
43. L. Wang, Y. D. Bi, J. Hou, H. Y. Li, Y. Xu, B. Wang, H. Ding, L. Ding, *Talanta.* **2016**, *160*, 268.
44. C. Barbosa, J. R. Correa, G. A. Medeiros, G. Barreto, K. G. Magalhaes, A. L. de Oliveira, J. Spencer, M. O. Rodrigues, B. A. D. Neto, *Chem-a Eur J*. **2015**, *21*, 5055.
45. R. L. Liu, J. Zhang, M. P. Gao, Z. L. Li, J. Y. Chen, D. Q. Wu, P. Liu, *RSC Adv.* **2015**, *5*, 4428.
46. J. Feng, W. J. Wang, X. Hai, Y. L. Yu, J. H. Wang, *J. Mater. Chem. B*. **2016**, *4*(, 387.
47. Q. Wang, X. Liu, L. C. Zhang, Y. Lv, *Analyst*. **2012**, *137*, 5392.
48. M. Farrell, D. L. Jones, *Bioresour. Technol.* **2009**, *100*, 4301.
49. J. Mata-Alvarez, S. Mace, P. Llabres, *Bioresour. Technol.* **2000**, *74*, 3.
50. Y. Y. Choi, S. R. Baek, J. I. Kim, J. W. Choi, J. Hur, T. U. Lee, C. J. Park, B. J. Lee, *Water.* **2017**, *9*, 409.
51. S. Devi, R. K. Gupta, A. K. Paul, V. Kumar, A. Sachdev, P. Gopinath, S. Tyagi, *RSC Adv.* **2018**, *8*, 32684.
52. A. A. Milrad, M. Ramadurai, S. Raghunandhakumar, S. G. Krishna, P. Prabhu, D. Anuradha, S. Abbas, *Colloids Surf., A.* **2020**, *586*, 124266.
53. S. W. Yang, J. Sun, X. B. Li, W. Zhou, Z. Y. Wang, P. He, G. Q. Ding, X. M. Xie, Z. H. Kang, M. H. Jiang, *J. Mater. Chem. A*. **2014**, *2*, 8660.

54. S. Thambiraj, D. R. Shankaran, *Appl. Surf. Sci.* **2016**, *390*, 435.
55. S. P. Sasikala, L. Henry, G. Y. Tonga, K. Huang, R. Das, B. Giroire, S. Marre, V. M. Rotello, A. Penicaud, P. Poulin, C. Aymonier, *ACS Nano*. **2016**, *10*, 5293.
56. J. B. Jia, Y. Sun, Y. J. Zhang, Q. R. Liu, J. L. Cao, G. X. Huang, B. L. Xing, C. X. Zhang, L. N. Zhang, Y. J. Cao, *Front Chem*. **2020**, *8*, 123.
57. Y. G. Tang, X. Huan, C. Y. Lan, M. X. Xu, *Acta Geologica Sinica-Engl Ed*. **2018**, *92*, 1218.
58. J. Yu, C. X. Zhang, Y. L. Yang, G. Y. Yi, R. Q. Fan, L. Li, B. L. Xing, Q. R. Liu, J. B. Jia, G. X. Huang, *New J. Chem.* **2019**, *43*, 18355.
59. L. Ding, K. T. Huang, S. A. Li, J. Zhou, H. He, Z. Z. Peng, S. Chatterjee, F. Liang, *J Fluoresc*. **2020**, *30*, 151.
60. M. B. Wu, Y. Wang, W. T. Wu, C. Hu, X. N. Wang, J. T. Zheng, Z. T. Li, B. Jiang, J. S. Qiu, *Carbon*. **2014**, *78*, 480.
61. X. T. Feng, Y. Zhang, *Rsc Advances.* **2019**, *9*, 33789.
62. M. Q. He, X. R. Guo, J. Z. Huang, H. H. Shen, Q. Zeng, L. S. Wang, *Carbon*. **2018**, *140*, 508.
63. Q. R. Liu, J. J. Zhang, H. He, G. X. Huang, B. L. Xing, J. B. Jia, C. X. Zhang, *Nanomaterials*. **2018**, *8*, 844.
64. P. H. Zhao, C. Z. Li, M. L. Yang, *J. Dispersion Sci. Technol.* **2017**, *38*, 769.
65. P. H. Zhao, Y. Luo, L. Y. Kong, *J Nano Res*. **2017**, *45*, 76.
66. L. Tian, D. Ghosh, W. Chen, S. Pradhan, X. J. Chang, S. W. Chen, *Chem. Mater.* **2009**, *21*, 2803.
67. P. Das, S. Ganguly, P. P. Maity, M. Bose, S. Mondal, S. Dhara, A. K. Das, S. Banerjee, N. C. Das, *J. Photochem. Photobiol. B, Biol.* **2018**, *180*, 56.
68. Y. Zhou, Y. Liu, Y. Q. Li, Z. Y. He, Q. Xu, Y. S. Chen, J. Street, H. Guo, M. Nelles, *RSC Adv.* **2018**, *8*, 23657.
69. B. Thangaraj, P. R. Solomon, S. Ranganathan, *Curr. Pharm. Des.* **2019**, *25*, 1455.
70. H. C. Liu, J. Ding, K. Zhang, L. Ding, *Trac-Trends Analyt Chem*. **2019**, *118*, 315.
71. N. A. Mahat, S. A. Shamsudin, *Diamond Relat. Mater.* **2020**, *102*, 107660.
72. D. Bano, V. Kumar, V. K. Singh, S. Chandra, D. K. Singh, P. K. Yadav, M. Talat, S. H. Hasan, *ACS Sustainable Chem. Eng.* **2019**, *7*, 1923.
73. P. Surendran, A. Lakshmanan, G. Vinitha, G. Ramalingam, P. Rameshkumar, *Luminescence.* **2020**, *35*, 196.
74. V. Ramar, S. Moothattu, K. Balasubramanian, *Sol. Energy*. **2018**, *169*, 120.
75. V. Singh, K. S. Rawat, S. Mishra, T. Baghel, S. Fatima, A. A. John, N. Kalleti, D. Singh, A. Nazir, S. K. Rath, A. Goel, *J. Mater. Chem. B*. **2018**, *6*, 3366.
76. S. Liu, J. Q. Tian, L. Wang, Y. W. Zhang, X. Y. Qin, Y. L. Luo, A. M. Asiri, A. O. Al-Youbi, X. P. Sun, *Adv. Mater.* **2012**, *24*, 2037.
77. S. A. A. Vandarkuzhali, V. Jeyalakshmi, G. Sivaraman, S. Singaravadivel, K. R. Krishnamurthy, B. Viswanathan, *Sens Actuators B Chem*. **2017**, *252*, 894.
78. L. S. Li, X. Y. Jiao, Y. Zhang, C. Cheng, K. Huang, L. Xu, *Sens Actuators B Chem*. **2018**, *263*, 426.
79. A. Kumar, A. R. Chowdhuri, D. Laha, T. K. Mahto, P. Karmakar, S. K. Sahu, *Sens Actuators B Chem*. **2017**, *242*, 679.
80. J. R. Bhamore, S. Jha, R. K. Singhal, T. J. Park, S. K. Kailasa, *J. Mol. Liq.* **2018**, *264*, 9.
81. R. Bandi, R. Dadigala, B. R. Gangapuram, V. Guttena, *J. Photochem. Photobiol. B, Biol.* **2018**, *178*, 330.
82. L. L. Yang, X. Sun, D. Li, C. H. Qu, H. L. Liu, M. B. Wei, X. Y. Liu, J. H. Yang, *Physica Status Solidi a-Applications and Materials Science*. **2019**, *216*, 1800404.
83. J. J. Zhang, Q. R. Liu, H. He, F. Shi, G. X. Huang, B. L. Xing, J. B. Jia, C. X. Zhang, *Carbon*. **2019**, *152*, 284.
84. L. P. Li, R. P. Zhang, C. X. Lu, J. H. Sun, L. J. Wang, B. T. Qu, T. T. Li, Y. D. Liu, S. J. Li, *J. Mater. Chem. B*. **2017**, *5*, 7328.
85. C. G. Cheng, Y. N. Shi, M. Li, M. Xing, Q. L. Wu, *Mater Sci Eng C Mater Biol Appl*. **2017**, *79*, 473.
86. P. Brachi, *Appl. Catal. B*. **2020**, *263*, 118361.
87. H. Kalita, J. Mohapatra, L. Pradhan, A. Mitra, D. Bahadur, M. Aslam, *RSC Adv.* **2016**, *6*, 23518.
88. P. Devi, G. Kaur, A. Thakur, N. Kaur, A. Grewal, P. Kumar, *Talanta*. **2017**, *170*, 49.
89. R. D. da Costa, W. F. da Cunha, N. S. Pereira, A. M. Ceschin, *Materials*. **2018**, *11*(9).
90. S. S. Jones, P. Sahatiya, S. Badhulika, *New J. Chem.* **2017**, *41*, 13130.
91. N. Murugan, M. Prakash, M. Jayakumar, A. Sundaramurthy, A. K. Sundramoorthy, *Appl. Surf. Sci.* **2019**, *476*, 468.
92. S. Y. Park, H. U. Lee, E. S. Park, S. C. Lee, J. W. Lee, S. W. Jeong, C. H. Kim, Y. C. Lee, Y. S. Huh, J. Lee, *ACS Appl. Mater. Interfaces*. **2014**, *6*, 3365.
93. P. C. Hsu, Z. Y. Shih, C. H. Lee, H. T. Chang, *Green Chem.* **2012**, *14*(, 917.
94. S. S. Jing, Y. S. Zhao, R. C. Sun, L. X. Zhong, X. W. Peng, *ACS Sustainable Chem. Eng.* **2019**, *7*, 7833.
95. Y. S. Liu, Y. A. Zhao, Y. Y. Zhang, *Sens Actuators B Chem*. **2014**, *196*, 647.
96. Z. Lai, X. Y. Guo, Z. F. Cheng, G. H. Ruan, F. Y. Du, *Chemistryselect.* **2020**, *5*, 1956.
97. A. M. Su, Q. M. Zhong, Y. Y. Chen, Y. L. Wang, *Anal. Chim. Acta.* **2018**, *1023*, 115.
98. H. Yuan, X. Zhang, D. Li, Y. Chen, *Nano*. **2018**, *13*, 84.
99. R. Q. Bao, Z. Y. Chen, Z. W. Zhao, X. Sun, J. Y. Zhang, L. R. Hou, C. Z. Yuan, *Nanomaterials*. **2018**, *8*, 386.
100. A. Pramanik, S. Biswas, P. Kumbhakar, *Spectrochim Acta A Mol Biomol Spectrosc*. **2018**, *191*, 498.
101. K. Rajendran, N. Rajendiran, *Mater. Res. Express*. **2018**, *5*, 024008.
102. R. B. Wang, G. J. Xia, W. T. Zhong, L. Chen, L. H. Chen, Y. G. Wang, Y. G. Min, K. X. Li, *Green Chem.* **2019**, *21*, 3343.
103. L. Zhang, H. P. Wang, Q. Hu, X. Q. Guo, L. Li, S. M. Shuang, X. J. Gong, C. Dong, *Microchim. Acta*. **2019**, *186*, 506.
104. W. L. Wang, Z. F. Wang, J. J. Liu, Y. K. Peng, X. Y. Yu, W. X. Wang, Z. G. Zhang, L. Y. Sun, *Ind. Eng. Chem. Res.* **2018**, *57*, 9144.
105. Z. Ramezani, M. Qorbanpour, N. Rahbar, *Colloids Surf., A*. **2018**, *549*, 58.
106. O. Rop, J. Balik, V. Reznicek, T. Jurikova, P. Skardova, P. Salas, J. Sochor, J. Mlcek, D. Kramarova, *Czech J. Food Sci.* **2011**, *29*, 65.
107. M. Jahanbakhshi, B. Habibi, *Biosens. Bioelectron.* **2016**, *81*, 143.
108. H. J. Qi, M. Teng, M. Liu, S. X. Liu, J. Li, H. P. Yu, C. B. Teng, Z. H. Huang, H. Liu, Q. Shao, A. Umar, T. Ding, Q. Gao, Z. H. Guo, *J. Colloid Interface Sci.* **2019**, *539*, 332.

109. M. K. Kumawat, M. Thakur, R. B. Gurung, R. Srivastava, *Sci. Rep.* **2017**, *7*, 15858.
110. H. T. Li, Z. H. Kang, Y. Liu, S. T. Lee, *J. Mater. Chem.* **2012**, *22*, 24230.
111. S. J. Wang, Z. G. Chen, I. Cole, Q. Li, *Carbon.* **2015**, *82*, 304.
112. M. C. Lu, Y. X. Duan, Y. H. Song, J. S. Tan, L. Zhou, *J. Mol. Liq.* **2018**, *269*, 766.
113. T. Joko, M. Umehara, T. Murata, H. Etoh, K. Izumori, S. Tsuyumu, *J Plant Interact*. **2018**, *13*, 141.
114. D. G. Babar, S. K. Sonkar, K. M. Tripathi, S. Sarkar, *J. Nanosci. Nanotechnol.* **2014**, *14*, 2334.
115. J. Ahn, Y. Song, J. E. Kwon, S. H. Lee, K. S. Park, S. Kim, J. Woo, H. Kim, *Mater Sci Eng C Mater Biol Appl*. **2019**, *102*, 106.
116. R. K. Dhillon, S. Singh, R. Kumar, *Radiat. Meas.* **2012**, *47*, 1018.
117. P. H. Zhu, C. C. Parrish, J. A. Brown, *Aquaculture Int*. **2003**, *11*, 43.
118. Y. H. Liu, C. Zhu, Y. Gao, L. Yang, J. Y. Xu, X. T. Zhang, C. Lu, Y. F. Wang, Y. Z. Zhu, *Appl. Surf. Sci.* **2020**, *510*, 14543.
119. H. Liu, J. Ding, L. Chen, L. Ding, *J Photochem Photobiol A Chem*. **2020**, *400*, 112724.
120. R. Atchudan, T. Edison, S. Perumal, N. Muthuchamy, Y. R. Lee, *Fuel*. **2020**, *275*, 117821.
121. A. Pal, G. Natu, K. Ahmad, A. Chattopadhyay, *J. Mater. Chem. A*. **2018**, *6*, 4111.
122. J. H. Shen, Y. H. Zhu, C. Chen, X. L. Yang, C. Z. Li, *Chem. Commun.* **2011**, *47*, 2580.
123. L. Bao, C. Liu, Z. L. Zhang, D. W. Pang, *Adv. Mater.* **2015**, *27*, 1663.
124. K. P. Loh, Q. L. Bao, G. Eda, M. Chhowalla, *Nat. Chem.* **2010**, *2*, 1015.
125. X. Wang, L. Cao, S. T. Yang, F. S. Lu, M. J. Meziani, L. L. Tian, K. W. Sun, M. A. Bloodgood, Y. P. Sun, *Angew. Chem. Int. Ed.* **2010**, *49*, 5310.
126. S. Chaudhary, S. Kumar, B. Kaur, S. K. Mehta, *RSC Adv.* **2016**, *6*, 90526.
127. J. Zhu, F. Y. Zhu, X. N. Yue, P. R. Chen, Y. Sun, L. Zhang, D. D. Mu, F. Ke, *J. Nanomater.* **2019**, *2019*, 7965756.
128. P. H. Zhao, M. L. Yang, W. Y. Fan, X. J. Wang, F. L. Tang, C. P. Yang, X. W. Dou, S. Y. Li, Y. A. Wang, Y. W. Cao, *Part. Part. Syst. Charact.* **2016**, *33*, 635.
129. G. Wang, G. L. Guo, D. Chen, Z. D. Liu, X. H. Zheng, A. L. Xu, S. W. Yang, G. Q. Ding, *ACS Appl. Mater. Interfaces.* **2018**, *10*, 5750.
130. J. R. Bhamore, S. Jha, T. J. Park, S. K. Kailasa, *J. Photochem. Photobiol. B, Biol.* **2019**, *191*, 150.
131. Z. M. Markovic, M. Labudova, M. Danko, D. Matijasevic, M. Micusik, V. Nadazdy, M. Kovacova, A. Kleinova, Z. Spitalsky, V. Pavlovic, D. D. Milivojevic, M. Medic, B. M. T. Markovic, *ACS Sustainable Chem. Eng.* **2020**, *8*, 16327.
132. J. Zhou, X. Shan, J. Ma, Y. Gu, Z. Qian, J. Chen, H. Feng, *RSC Adv.* **2014**, *4*, 5465.
133. Y. Y. Liu, J. Zhang, X. Zhao, W. T. Li, J. Wang, Y. H. Gao, Y. Y. Cui, S. H. Xu, X. L. Luo, *Chem. Commun.* **2020**, *56*, 4074.
134. Z. L. Li, Y. Zhang, Q. Q. Niu, M. Y. Mou, Y. Wu, X. X. Liu, Z. Y. Yan, S. H. Liao, *J. Lumin*. **2017**, *187*, 274.
135. S. Sahu, B. Behera, T. K. Maiti, S. Mohapatra, *Chem. Commun.* **2012**, *48*, 8835.
136. H. Soni, P. S. Pamidimukkala, *Mater. Res. Bull.* **2018**, *108*, 250.
137. Z. Y. Chen, Z. W. Zhao, Z. L. Wang, Y. R. Zhang, X. Sun, L. R. Hou, C. Z. Yuan, *New J. Chem.* **2018**, *42*, 7326.
138. Y. X. Shi, X. Liu, M. Wang, J. B. Huang, X. Q. Jiang, J. H. Pang, F. Xu, X. M. Zhang, *Int. J. Biol. Macromol.* **2019**, *128*, 537.
139. X. Q. Jiang, Y. X. Shi, X. Liu, M. Wang, P. P. Song, F. Xu, X. M. Zhang, *Polymers*. **2018**, *10*, 1282.
140. Y. Lin, Y. H. Li, H. Yang, H. P. Huang, L. Li, S. X. Li, *Chinese J. Anal. Chem.* **2019**, *47*, 748.
141. X. Y. Deng, Y. L. Feng, H. R. Li, Z. W. Du, Q. Teng, H. J. Wang, *Particuology*. **2018**, *41*, 94.
142. D. Y. Yu, L. Wang, H. Y. Zhou, X. J. Zhang, L. Wang, N. Qiao, *Bioconjugate Chem.* **2019**, *30*, 966.
143. Y. Xu, Y. Fan, L. Zhang, Q. Wang, H. Y. Fu, Y. B. She, *Spectrochim Acta A Mol Biomol Spectrosc*. **2019**, *220*, 117109.
144. D. Wang, B. X. Lin, Y. J. Cao, M. L. Guo, Y. Yu, *J. Agric. Food Chem.* **2016**, *64*, 6042.
145. H. C. Daia, Y. Shi, Y. L. Wang, Y. J. Sun, J. T. Hu, P. J. Ni, Z. Li, *Sens Actuators B Chem.* **2014**, *202*, 201.
146. C. K. Jiang, H. Wu, X. J. Song, X. J. Ma, J. H. Wang, M. Q. Tan, *Talanta*. **2014**, *127*, 68.
147. A. Suryawanshi, M. Biswal, D. Mhamane, R. Gokhale, S. Patil, D. Guin, S. Ogale, *Nanoscale.* **2014**, *6*, 11664.
148. L. Wang, W. T. Li, B. Wu, Z. Li, S. L. Wang, Y. Liu, D. Y. Pan, M. H. Wu, *Chem. Eng. J.* **2016**, *300*, 75.
149. S. Y. Lim, W. Shen, Z. Q. Gao, *Chem. Soc. Rev.* **2015**, *44*, 362.
150. M. J. Molaei, *Talanta.* **2019**, *196*, 456.
151. Y. Tang, L. S. Rao, Z. T. Li, H. G. Lu, C. M. Yan, S. D. Yu, X. R. Ding, B. H. Yu, *Sens Actuators B Chem*. **2018**, *258*, 637.
152. X. D. Wu, B. Zhao, J. Z. Zhang, H. Xu, K. Q. Xu, G. Chen, *J. Phys. Chem. C*. **2019**, *123*, 25570.
153. C. Hu, C. Yu, M. Y. Li, X. N. Wang, J. Y. Yang, Z. B. Zhao, A. Eychmuller, Y. P. Sun, J. S. Qiu, *Small*. **2014**, *10*, 4926.
154. Z. X. Liu, H. Y. Zou, N. Wang, T. Yang, Z. W. Peng, J. Wang, N. Li, C. Z. Huang, *Sci China Chem*. **2018**, *61*, 490.
155. C. L. Wang, J. Xu, H. Z. Li, W. L. Zhao, *Luminescence*, https://doi.org/10.1002/bio.3901.
156. J. Zhang, H. Wang, Y. M. Xiao, J. Tang, C. N. Liang, F. Y. Li, H. M. Dong, W. Xu, *Nanoscale Res. Lett.* **2017**, *12*, 1.
157. Z. H. Wen, X. B. Yin, *RSC Adv.* **2016**, *6*, 27829.
158. S. Kim, S. W. Hwang, M. K. Kim, D. Y. Shin, D. H. Shin, C. O. Kim, S. B. Yang, J. H. Park, E. Hwang, S. H. Choi, G. Ko, S. Sim, C. Sone, H. J. Choi, S. Bae, B. H. Hong, *ACS Nano*. **2012**, *6*, 8203.
159. S. J. Zhu, L. Wang, B. Li, Y. B. Song, X. H. Zhao, G. Y. Zhang, S. T. Zhang, S. Lu, J. H. Zhang, H. Y. Wang, H. B. Sun, B. Yang, *Carbon.* **2014**, *77*, 462.
160. Y. Z. Zhu, M. Qiao, W. C. Peng, Y. Li, G. L. Zhang, F. B. Zhang, Y. F. Li, X. B. Fan, *J. Mater. Chem. A*. **2017**, *5*, 9272.
161. J. H. Shen, Y. H. Zhu, X. L. Yang, C. Z. Li, *Chem. Commun.* **2012**, *48*, 3686.
162. W. Kwon, Y. H. Kim, C. L. Lee, M. Lee, H. C. Choi, T. W. Lee, S. W. Rhee, *Nano Lett.* **2014**, *14*, 1306.
163. X. Y. Tan, Y. C. Li, X. H. Li, S. X. Zhou, L. Z. Fan, S. H. Yang, *Chem. Commun.* **2015**, *51*, 2544.
164. J. Yang, W. L. Chen, X. P. Liu, Y. Zhang, Y. Bai, *Mater. Res. Bull.* **2017**, *89*, 26.
165. Q. Q. Fang, Y. Q. Dong, Y. M. Chen, C. H. Lu, Y. W. Chi, H. H. Yang, T. Yu, *Carbon.* **2017**, *118*, 319.
166. S. K. Kailasa, S. Ha, S. H. Baek, L. M. T. Phan, S. Kim, K. Kwak, T. J. Park, *Mater Sci Eng C Mater Biol Appl*. **2019**, *98*, 834.

167. C. J. Jeong, A. K. Roy, S. H. Kim, J. E. Lee, J. H. Jeong, I. In, S. Y. Park, *Nanoscale*. **2014**, *6*, 15196.
168. X. J. Gong, W. J. Lu, Y. Liu, Z. B. Li, S. M. Shuang, C. Dong, M. M. F. Choi, *J. Mater. Chem. B*. **2015**, *3*, 6813.
169. W. D. Li, Y. Liu, B. Y. Wang, H. Q. Song, Z. Y. Liu, S. Y. Lu, B. Yang, *Chin. Chem. Lett.* **2019**, *30*, 2323.
170. G. S. Das, J. P. Shim, A. Bhatnagar, K. M. Tripathi, T. Kim, *Sci. Rep.* **2019**, *9*, 15084.
171. L. G. Zhang, Y. Wang, W. Liu, Y. H. Ni, Q. X. Hou, *Ind. Crops Prod.* **2019**, *133*, 18.
172. L. Xu, W. Mao, J. R. Huang, S. H. Li, K. Huang, M. Li, J. L. Xia, Q. Chen, *Sens Actuators B Chem*. **2016**, *230*, 54.
173. Z. Khan, R. S. Rahman, Shumaila, S. Islam, M. Zulfequar, *Opt Mater (Amst)*. **2019**, *91*, 386.
174. Q. C. Zhang, X. L. Zhang, L. C. Bao, Y. Wu, L. Jiang, Y. G. Zheng, Y. Wang, Y. F. Chen, *J. Anal. Methods Chem.* **2019**, *2019*, 8183134.
175. N. Pourreza, M. Ghomi, *Mater Sci Eng C Mater Biol Appl*. **2019**, *98*, 887.
176. S. Chandra, V. K. Singh, P. K. Yadav, D. Bano, V. Kumar, V. K. Pandey, M. Talat, S. H. Hasan, *Anal. Chim. Acta.* **2019**, *1054*, 145.
177. P. K. Yadav, V. K. Singh, S. Chandra, D. Bano, V. Kumar, M. Talat, S. H. Hasan, *ACS Biomater. Sci. Eng.* **2019**, *5*, 623.
178. H. Xue, Y. Yan, Y. Hou, G. L. Li, C. Hao, *New J. Chem.* **2018**, *42*, 11485.
179. H. Miao, Y. Y. Wang, X. M. Yang, *Nanoscale*. **2018**, *10*, 8139.
180. A. Iqbal, Y. J. Tian, X. D. Wang, D. Y. Gong, Y. L. Guo, K. Iqbal, Z. P. Wang, W. S. Liu, W. W. Qin, *Sens Actuators B Chem*. **2016**, *237*, 408.
181. X. Y. Zhao, S. Liao, L. M. Wang, Q. Liu, X. Q. Chen, *Talanta.* **2019**, *201*, 1.
182. C. J. Wang, H. X. Shi, M. Yang, Y. J. Yan, E. Z. Liu, Z. Ji, J. Fan, *Mater. Res. Bull.* **2020**, *124*, 110730.
183. B. H. Luo, H. Yang, B. X. Zhou, S. M. Ahmed, Y. Zhang, H. M. Liu, X. W. Liu, Y. He, S. B. Xia, *ACS Omega*. **2020**, *5*, 5540.
184. A. Diac, M. Focsan, C. Socaci, A. M. Gabudean, C. Farcau, D. Maniu, E. Vasile, A. Terec, L. M. Veca, S. Astilean, *RSC Adv.* **2015**, *5*, 77662.
185. Z. C. Liang, M. J. Kang, G. F. Payne, X. H. Wang, R. C. Sun, *ACS Appl. Mater. Interfaces*. **2016**, *8*, 17478.
186. H. B. Liu, C. Y. Xu, Y. L. Bai, L. Liu, D. M. Liao, J. G. Liang, L. Z. Liu, H. Y. Han, *Spectrochim Acta A Mol Biomol Spectrosc*. **2017**, *171*, 311.
187. X. Sun, Y. R. Liu, N. Niu, L. G. Chen, *Anal. Bioanal. Chem.* **2019**, *411*, 5519.
188. A. Chatzimarkou, T. G. Chatzimitakos, A. Kasouni, L. Sygellou, A. Avgeropoulos, C. D. Stalikas, *Sens Actuators B Chem*. **2018**, *258*, 1152.
189. J. J. Liu, Y. L. Chen, W. F. Wang, J. Feng, M. J. Liang, S. D. Ma, X. G. Chen, *J. Agric. Food Chem.* **2016**, *64*, 371.
190. J. Singh, S. Kaur, J. Lee, A. Mehta, S. Kumar, K. H. Kim, S. Basu, M. Rawat, *Sci. Total Environ.* **2020**, *720*, 137604.
191. T. Chatzimitakos, A. Kasouni, L. Sygellou, A. Avgeropoulos, A. Troganis, C. Stalikas, *Talanta.* **2017**, *175*, 305.
192. S. Bhatt, M. Bhatt, A. Kumar, G. Vyas, T. Gajaria, P. Paul, *Colloids Surf B Biointerfaces*. **2018**, *167*, 126.
193. B. Mistry, H. K. Machhi, R. S. Vithalani, D. S. Patel, C. K. Modi, M. Prajapati, K. R. Surati, S. S. Soni, P. K. Jha, S. R. Kane, *Sustainable Energy Fuels*. **2019**, *3*, 3182.
194. B. H. Zhang, Y. J. Liu, M. Q. Ren, W. T. Li, X. Zhang, R. Vajtai, P. M. Ajayan, J. M. Tour, L. Wang, *Chemsuschem.* **2019**, *12*, 4202.
195. X. Gao, X. D. Ji, T. T. Nguyen, X. C. Gong, R. S. Chai, M. H. Guo, *Vacuum.* **2019**, *164*, 256.
196. A. M. Su, D. Wang, X. Shu, Q. M. Zhong, Y. R. Chen, J. C. Liu, Y. L. Wang, *Chem. Res. Chin. Univ.* **2018**, *34*, 164.
197. D. Rodriguez-Padron, M. Algarra, L. A. C. Tarelho, J. Frade, A. Franco, G. de Miguel, J. Jimenez, E. Rodriguez-Castellon, R. Luque, *ACS Sustainable Chem. Eng.* **2018**, *6*, 7200.
198. Q. M. Yang, J. L. Duan, W. Yang, X. M. Li, J. H. Mo, P. Z. Yang, Q. W. Tang, *Appl. Surf. Sci.* **2018**, *434*, 1079.
199. X. Y. Chai, H. He, H. H. Fan, X. H. Kang, X. P. Song, *Bioresour. Technol.* **2019**, *282*, 142.
200. W. F. Chen, J. L. Shen, G. Lv, D. J. Li, Y. L. Hu, C. L. Zhou, X. Liu, Z. X. Dai, *Chemistryselect.* **2019**, *4*, 2898.
201. H. Teymourinia, M. Salavati-Niasari, O. Amiri, H. Safardoust-Hojaghan, *J. Mol. Liq.* **2017**, *242*, 447.
202. M. K. Kumawat, M. Thakur, R. B. Gurung, R. Srivastava, *ACS Sustainable Chem. Eng.* **2017**, *5*, 1382.
203. P. Roy, R. Ravindranath, A. P. Periasamy, C. W. Lien, C. T. Liang, H. T. Chang, *RSC Adv.* **2016**, *6*, 108941.
204. Z. F. Wang, J. F. Yu, X. Zhang, N. Li, B. Liu, Y. Y. Li, Y. H. Wang, W. X. Wang, Y. Z. Li, L. C. Zhang, S. Dissanayake, S. L. Suib, L. Y. Sun, *ACS Appl. Mater. Interfaces*. **2016**, *8*, 1434.
205. Q. H. Liang, W. J. Ma, Y. Shi, Z. Li, X. M. Yang, *Carbon*. **2013**, *60*, 421.
206. X. M. Yang, Y. Zhuo, S. S. Zhu, Y. W. Luo, Y. J. Feng, Y. Dou, *Biosens. Bioelectron.* **2014**, *60*, 292.
207. L. H. Shi, B. Zhao, X. F. Li, G. M. Zhang, Y. Zhang, C. Dong, S. M. Shuang, *Sens Actuators B Chem*. **2016**, *235*, 316.
208. Y. L. Cheng, M. S. Bai, J. Su, C. Q. Fang, H. Li, J. Chen, J. M. Jiao, *J. Mater. Sci. Technol.* **2019**, *35*, 1515.
209. M. Varisco, D. Zufferey, A. Ruggi, Y. C. Zhang, R. Erni, O. Mamula, *R. Soc. Open Sci.* **2017**, *4*, 170900.
210. R. M. Shereema, T. V. Sruthi, V. B. S. Kumar, T. P. Rao, S. S. Shankar, *Biochemistry*. **2015**, *54*, 6352.
211. K. Sarkar, P. Devi, A. Lata, R. Ghosh, P. Kumar, *J. Mater. Chem. C*. **2019**, *7*, 13182.
212. H. B. Feng, H. W. Dong, B. F. Lei, Y. Xiao, H. Hu, H. R. Zhan, Y. L. Liu, M. T. Zheng, *Sci. Adv. Mater.* **2016**, *8*, 948.
213. J. Dai, Y. J. Wang, *Appl. Ecol. Env. Res.* **2019**, *17*, 12139.
214. B. Rooj, A. Dutta, S. Islam, U. Mandal, *J Fluoresc*. **2018**, *28*, 1261.
215. N. Arumugam, J. Kim, *Mater. Lett.* **2018**, *219*, 37.
216. D. Bano, V. Kumar, V. K. Singh, S. H. Hasan, *New J. Chem.* **2018**, *42*, 5814.
217. Y. L. Liu, Q. X. Zhou, J. Li, M. Lei, X. Y. Yan, *Sens Actuators B Chem*. **2016**, *237*, 597.
218. J. Yu, N. Song, Y. K. Zhang, S. X. Zhong, A. J. Wang, J. R. Chen, *Sens Actuators B Chem*. **2015**, *214*, 29.
219. D. Gu, S. M. Shang, Q. Yu, J. Shen, *Appl. Surf. Sci.* **2016**, *390*, 38.
220. A. Tyagi, K. M. Tripathi, N. Singh, S. Choudhary, R. K. Gupta, *RSC Adv.* **2016**, *6*, 72423.
221. R. Atchudan, T. Edison, K. R. Aseer, S. Perumal, N. Karthik, Y. R. Lee, *Biosens. Bioelectron.* **2018**, *99*, 303.
222. T. Edison, R. Atchudan, J. J. Shim, S. Kalimuthu, B. C. Ahn, Y. R. Lee, *J. Photochem. Photobiol. B, Biol.* **2016**, *158*, 235.
223. S. Singh, P. Nigam, A. Pednekar, S. Mukherjee, A. Mishra, *Environ. Technol.* **2020**, *41*, 322.

224. K. J. Wang, Q. J. Ji, J. L. Xu, H. X. Li, D. Y. Zhang, X. Y. Liu, Y. J. Wu, H. Y. Fan, *J Fluoresc*. **2018**, *28*, 759.
225. A. A. Ensafi, P. Nasr-Esfahani, B. Rezaei, *Sens Actuators B Chem*. **2018**, *257*, 889.
226. J. Sun, Y. Z. He, L. Wang, *Anal. Methods*. **2017**, *9*, 3525.
227. H. Xu, X. P. Yang, G. Li, C. Zhao, X. J. Liao, *J. Agric. Food Chem.* **2015**, *63*, 6707.
228. H. Miao, L. Wang, Y. Zhuo, Z. N. Zhou, X. M. Yang, *Biosens. Bioelectron.* **2016**, *86*, 83.

How to cite this article: Lou Y, Hao X, Liao L, et al. Recent advances of biomass carbon dots on syntheses, characterization, luminescence mechanism, and sensing applications. *Nano Select*. 2021;1-29. https://doi.org/10.1002/nano.202000232